Spatial pattern formation and delay induced destabilization in predator-prey model with fear effect

Swati Mishra, Ranjit Kumar Upadhyay*

Department of Mathematics & computing, Indian Institute of Technology (ISM), Dhanbad 826004, Jharkhand, India

Abstract

Recent field experiments showed that predators influence the prey population not only by direct consumption but also by stimulating various defensive strategies. The cost of these defensive strategies can include energetic investment in defensive structures, reduced energy income, lower mating success, and emigration which ultimately reduces the reproduction of prey. To explore the effect of these defensive strategies (anti-predator behaviors), a modified Leslie-Gower predator-prey model with the cost of fear has been considered. Gestation delay is also incorporated in the system for a more realistic formulation. Boundedness, equilibria and stability analysis of the temporal model are studied. By considering gestation delay as a bifurcation parameter, the existence of Hopf-bifurcation around the interior equilibrium point is discussed together with the direction, stability and period of bifurcating solutions arising through Hopf-bifurcation. The spatial extension of the proposed model incorporating density-dependent cross-diffusion is also investigated and the conditions for diffusion-driven instability are obtained. To illustrate the analytical findings, detailed numerical simulations are performed. Biologically realistic Turing patterns as hexagonal spots, spots and stripes mixture, and labyrinthine type patterns are identified. It is found that the fear level has a stabilizing impact on delay induced destabilization and both stabilizing and destabilizing effects on Turing instability.

Keywords: Fear effect, gestation delay, cross-diffusion, Hopf-bifurcation, Turing instability
MSC: 92D40, 92D25, 35B36, 35K57, 70K05

1. Introduction

Predation is a central component of ecological communities. In predator-prey interactions, the main attention has been given to the lethal effects of predators, while the nonlethal effects of predators have received much less attention [1, 2]. In the presence of predators, prey exhibits various behavioral responses to predation risk including changes in habitat use [3, 4], movement patterns [5, 6], vigilance [7, 8], escape distance [9], and foraging behavior [10, 11]. These responses lead to a lot of energy investment in defensive structures, reduction in energy income, lower mating success and make them more vulnerable towards the other predators [12]. The most clear demonstration of these effects is a substantial impact on prey reproduction and population demography caused by predators. These processes occur on a large time scale and traditionally, it has been mistaken that these processes are the result of a shortage of food or parasitic infection [13].

Recent experimental developments have shown that nonlethal effects (risk effects) can be as large or even larger than the lethal effects (direct effects) [6, 14, 12]. Schmitz et al. [6] have demonstrated that risk spiders caused the same level of grasshopper (Melanoplus femurrubrum)

*Corresponding author
Email addresses: swatiiiitismsept2015@gmail.com (Swati Mishra), ranjit.chaos@gmail.com (Ranjit Kumar Upadhyay)

mortality as normal lethal spiders (Pisurina mira). The demography of mayflies without predators (stoneflies) and with nonlethal or untreated predators (gluing together their mouthparts) have been compared by Peckarsky et al. [15]. They have reported that nonlethal predators affect the variety of species and from meta-analysis of existing literature, they have suggested that 'intimidation' by predators can impact the prey demography more strongly than direct predation [12, 13]. Pangle et al. [14] have conducted an experiment on predatory spiny water fleas (Bythotrephes longimanus) and on three species of zooplankton in Lake Michigan and Lake Erie. They have found that over six combinations of location and depth, risk effects on population growth rates were more than seven times larger than the direct effects of predation. Zanette et al. [16] have performed a field experiment on song sparrows by actively preventing the direct predation using the electric fences and seines throughout the entire breeding season of 130 days. They have managed the predator risk by using the predator call playbacks and reported a 40% reduction in the number of offspring produced per year by wild free-living female song sparrows.

Based on the above field demonstrations, fear effect in the mathematical model of predator-prey interactions was first incorporated by Wang et al. [17]. After that various studies such as fear effect with prey refuge, adaptive avoidance of predators, multiple Allee effects, fear-induced trophic cascade, pattern formation with the cost of anti-predator behaviors, and fearful prey in a spatiotemporal system [18, 19, 20, 21, 22, 23, 24] have been carried out.

Time delays are ubiquitous in all biological situations as various biological processes such as digestion, gestation, maturation, and incubation are not instantaneous. However, species require some time in order to complete these biological activities. Time delay models are much more realistic in nature. In this work, we have assumed that the reproduction of predators after consuming the prey is not instantaneous, however, it is mediated by some time lag, called gestation delay. Predator-prey models with gestation delays have been studied by many researchers [25, 26, 27, 28]. Recently, the effect of delay on the population model with the cost of indirect effects has received the attention of many researchers. Panday et al. [29] have shown the stability switching behavior and chaos in a population model with delay and fear effect. Fear effects in a predator-prey model with gestation delay and prey refuse have been studied by Kumar and Dubey [30]. Duan et al. [31] have discussed the delayed diffusive model with fear effect.

Predator species have natural proclivity to move and catch the prey species while prey species have natural tendency to move away from predator species to avoid predation. Also, the movement of predator species depends on many factors like the presence, absence, abundance and scarcity of prey species and vice-versa. This identifiable information is called cross-diffusion which was first proposed by Kerner [32, 33] and used by Shigesada et al. [34] in a competitive population system. After this pioneer work, many researchers have studied the spatiotemporal dynamics of a predator-prey system with linear and nonlinear cross-diffusion terms [35, 36, 37, 38]. All these studies considered only the direct effects of predators. Recently, [39] have investigated a predator-prey model with linear cross-diffusion and fear effects. They have studied the cross-diffusion-driven Turing instability, pattern formation and pattern selection using the amplitude equations. Han et al. [40] have discussed the cross-diffusion-induced pattern formation and pattern selection in a modified Leslie-Gower(LG) model with fear effect. In this work, we have explored the dynamics of a predator-prey system with fear effects and nonlinear cross-diffusion.

In the present work, we have analyzed how fear influences the temporal, delayed, and the spatiotemporal dynamics of a two species predator-prey model with Crowley-Martin functional response. The cost of defensive strategies (due to fear of predators) is incorporated by multiplying the growth term of prey by the factor $\frac{1}{1+ky}$. It is found that the fear level k has a stabilizing effect on the temporal dynamics as well as on delay induced destabilization. The fear level k has both stabilizing and destabilizing effects on Turing instability. Hexagonal hot and cold spot patterns appear which changes to mixture of spots and stripes, and then to Labyrinthine patterns with change in the cross-diffusion coefficient of prey. Paper is organized as follows: In Section 2, we have presented the formulation of temporal and delay model systems incorporating the cost of defensive strategies

due to fear. Analysis of the temporal model system is carried out with boundedness, equilibria and stability analysis in Section 3. In section 4, linear stability analysis of the delay system via Hopf-bifurcation has been studied. The formulae for direction and stability of bifurcating periodic solutions arising through Hopf-bifurcation are also derived. The spatially explicit model system is discussed in the next section 5. Stability analysis and cross-diffusion induced Turing instability conditions are obtained. In Section 6, analytical results are validated through numerical simulations. Discussions and conclusions on the analytical and numerical findings are presented in the last section.

2. Model formulation

In the present work, we have considered a modified Leslie–Gower type predator-prey model with Crowley-Martin functional response [41]

$$\begin{aligned} \frac{dx}{dt} &= ax - dx^2 - \frac{wxy}{(1+\alpha x)(1+\beta y)}, \\ \frac{dy}{dt} &= sy - \frac{hy^2}{x+b}, \end{aligned} \tag{1}$$

where $x(t)$ and $y(t)$ denote the population densities of prey and predator respectively at any time t, $a,\ d,\ w,\ \alpha,\ \beta,\ s,\ h,\ b$ are positive constants and their biological meanings are given in Table 1. The underlying assumptions of above model formulation are as follows:

(i) In the absence of predator y, prey x is growing logistically with intrinsic growth rate a and carrying capacity a/d such that $\frac{dx}{dt} = ax - dx^2 = ax(1 - \frac{x}{a/d})$.

(ii) The predator y is of generalist type whose most favourite food is prey x. Predator y is consuming prey x with Crowley-Martin (C-M) functional response. C-M functional response is a predator dependent functional response and per capita feeding rate of predator y in this formulation is $\frac{wxy}{(1+\alpha x)(1+\beta y)}$.

(iii) The predator y does not follow the "mass conservation" principle, however introduce a modified Leslie-Gower term $\frac{hy}{x+b}$.

Recent field experiments [16] have demonstrated that the fear may influence the prey reproduction. To incorporate the impact of fear, we modify the model system (1) by multiplying the growth term ax of prey by the factor $F(k;y) = \frac{1}{1+ky}$, which incorporates the cost of defensive strategies due to fear. The parameter k reflects the level of fear which drives the anti-predator behaviors (defensive behaviors) in prey. It is assumed that scared prey forage less and left their newborn less protected, which in turn reduces the growth rate of prey. Under above assumptions the model system (1) takes the following form:

$$\begin{aligned} \frac{dx}{dt} &= \frac{ax}{1+ky} - dx^2 - \frac{wxy}{(1+\alpha x)(1+\beta y)}, \\ \frac{dy}{dt} &= sy - \frac{hy^2}{x+b}. \end{aligned} \tag{2}$$

The function $F(k;y) = \frac{1}{1+ky}$ is biologically suitable to incorporate the cost of anti-predator behaviours due to fear as it satisfies the following:

(a) $F(0;y) = 1$: If fear level $k = 0$ i.e., no defensive strategies then no reduction in the prey reproduction.

(b) $F(k;0) = 1$: In the absence of predator, no reduction in prey reproduction due to defensive strategies.

(c) $\lim_{k\to\infty} F(k,y) = 0$: If fear level is very high then prey production reduces to zero due to costly defensive strategies.

(d) $\lim_{y\to\infty} F(k,y) = 0$: If predator density is very high then foraging activities of prey are almost zero thus prey production reduces to zero.

(e) $\frac{\partial F(k,S)}{\partial k} < 0$: The production of prey decreases with an increase costly defensive strategies.

(f) $\frac{\partial F(k,S)}{\partial y} < 0$:The production of prey decreases with an increase in the predator population size due to impaired foraging activities.

The reproduction of the predator population after predating the prey is not a simultaneous process, however, it is mediated by some constant time lag $\tau > 0$ required for the gestation of predator. Now, incorporating the delay τ into the model system (2), we obtain the following system of DDEs:

$$\begin{aligned} \frac{dx}{dt} &= \frac{ax}{1+ky} - dx^2 - \frac{wxy}{(1+\alpha x)(1+\beta y)}, \\ \frac{dy}{dt} &= sy - \frac{hy^2(t-\tau)}{x(t-\tau)+b}. \end{aligned} \tag{3}$$

3. Analysis of the temporal model

3.1. Boundedness and positivity

Boundedness and positivity of the model system (2) have been studied in this subsection.

Theorem 3.1. *The solution of the model system* (2) *are positive and eventually bounded i.e. there exist* $T \geq 0$ *such that* $x(t) < M_1$ *and* $y(t) < M_2,\ \forall t \geq T$.

Proof. The phase diagram of the system (2) is presented in Fig. 1. For the system (2), nullclines are $C_1 : y = \frac{-q \pm \sqrt{q^2-4pr}}{2p},\ p = wk + d\beta kx(1+\alpha x), \quad q = w + \beta(dx-a)(1+\alpha x) + dkx(1+\alpha x)$, $r = (dx-a)(1+\alpha x)$ on which $\frac{dx}{dt} = 0$; and $C_2 : y = \frac{s(x+b)}{h}$, on which $\frac{dy}{dt} = 0$. C_1 and C_2 partition the first quadrant into four parts $D_1,\ D_2,\ D_3$, and D_4. The intersection of C_1 and C_2 is the unique interior equilibrium point $E^*(x^*, y^*)$. Set $L_1 = \{(x,y) \mid x = M_1,\ 0 \leq y \leq M_2\}$ and $L_2 = \{(x,y) \mid 0 \leq x \leq M_1,\ y = M_2\}$. The rectangular region consisting of $L_1,\ L_2,\ y-$ axis and $x-$ axis as boundaries is denoted by $D\ (= D_1 \cup D_2 \cup D_3 \cup D_4)$. It is clear that D is an invariant set and attracts any trajectory starting in the first quadrant. Thus, solution of the system (2) are eventually bounded.

Next, we have discussed the positivity of the solution of the system (2). For this, we have shown that any trajectory starting in first quadrant cannot reach the y-axis. To this end, we only need to prove that trajectory cannot arrive the y-axis in D_2. From a given point $(x_0, y_0) \in D_2$, the time of a trajectory running from (x_0, y_0) to C_1 is denoted by T_1 and $T_2(N)$ is the time of trajectory running from (x_0, y_0) to $\frac{x_0}{N}$, $N \in \mathbb{N}$, $N \geq 2$. We estimate the times T_1 and T_2.

$$T_1 \leq \int_{y_0}^{0.6} \frac{dy}{y\left(s - \frac{hy}{(x+b)}\right)} \leq \int_{0.6}^{y_0} \frac{dy}{y\left(\frac{hy}{(x_0+b)} - s\right)} = \frac{1}{s} ln\left(\frac{3h - \frac{3s(x_0+b)}{y_0}}{3h - 5s(x_0+b)}\right). \tag{4}$$

Hence T_1 is finite. Now,

$$T_2(N) = \int_{x_0}^{x_0/N} \frac{dx}{\frac{ax}{1+ky} - dx^2 - \frac{wxy}{(1+\alpha x)(1+\beta y)}} = \int_{x_0/N}^{x_0} \frac{dx}{\left(-\frac{ax}{1+ky} + dx^2 + \frac{wxy}{(1+\alpha x)(1+\beta y)}\right)}$$
$$\geq \int_{x_0/N}^{x_0} \frac{dx}{x(-\frac{a}{1+ky_0} + dx + \frac{w}{\beta})} \tag{5}$$
$$= \frac{1}{\left(-\frac{a}{1+ky_0} + \frac{w}{\beta}\right)} ln \left\{ \frac{dx_0 + N\left(-\frac{a}{1+ky_0} + \frac{w}{\beta}\right)}{-\frac{a}{1+ky_0} + dx_0 + \frac{w}{\beta}} \right\}.$$

Since

$$\lim_{N\to\infty} \frac{1}{\left(-\frac{a}{1+ky_0} + \frac{w}{\beta}\right)} ln \left\{ \frac{dx_0 + N\left(-\frac{a}{1+ky_0} + \frac{w}{\beta}\right)}{-\frac{a}{1+ky_0} + dx_0 + \frac{w}{\beta}} \right\} = \infty, \tag{6}$$

therefore $\exists$ some $N_0 \in \mathbb{N}$ such that

$$\frac{1}{\left(-\frac{a}{1+ky_0} + \frac{w}{\beta}\right)} ln \left\{ \frac{dx_0 + N_0\left(-\frac{a}{1+ky_0} + \frac{w}{\beta}\right)}{-\frac{a}{1+ky_0} + dx_0 + \frac{w}{\beta}} \right\} > \frac{1}{s} ln \left(\frac{3h - \frac{3s(x_0+b)}{y_0}}{3h - 5s(x_0+b)} \right). \tag{7}$$

Hence $T_2(N_0) > T_1$. Thus, time of trajectory to reach the y-axis is far longer than that to C_1, i.e., trajectory runs into D_3 before reaching to the y-axis. From the properties of vector field shown in Fig. 1, the trajectory cannot reach the y-axis in D_3. Therefore, any trajectory starting in the first quadrant cannot reach the y-axis.From the above discussion, we know that there is no homoclinic or heteroclinic orbit in the domain D. Hence, it is proved. □

3.2. Equilibria and stability analysis

The equilibrium points of system (2) include trivial equilibrium $E_0(0,0)$, predator free equilibrium $E_1(\frac{a}{d},0)$, prey free equilibrium $E_2(0,\frac{bs}{h})$ and interior equilibrium $E^*(x^*,y^*)$. $E^*(x^*,y^*)$ is obtained by solving the system

$$\begin{aligned} \frac{a}{1+ky} - dx - \frac{wy}{(1+\alpha x)(1+\beta y)} &= 0, \\ s - \frac{hy}{(x+b)} &= 0. \end{aligned} \tag{8}$$

Solving second equation of the above system for y, we have $y = \frac{s(x+b)}{h}$. Now, putting the above value of y in the first equation of the system (8) and after simple calculations, x^* is given by the following equation

$$P_4x^4 + P_3x^3 + P_2x^2 + P_1x + P_0 = 0, \tag{9}$$

where

$$\begin{aligned} P_4 &= dks^2\alpha\beta, \\ P_3 &= ds(ks(1+2b\alpha)\beta + h\alpha(k+\beta)), \\ P_2 &= s(ksw - ah\alpha\beta) + d(h^2\alpha + bks^2(2+b\alpha)\beta + hs(1+b\alpha)(k+\beta)), \\ P_1 &= 2bks^2w - ah^2\alpha + d(h+bks)(h+bs\beta) + hs(w - a(1+b\alpha)\beta), \\ P_0 &= bs(h+bks)w - ah(h+bs\beta). \end{aligned}$$

Clearly, P_4 and P_3 are positive. Thus, the number of possible positive real roots of the Eq. (9) can be decided on the basis of the signs of P_2, P_1 and P_0. Various possibilities of positive real roots of

Eq. (9) are investigated by applying the Descartes rule of signs. All these possibilities are tabulated in Table 2. From Table 2, we can conclude that the Eq. (9) has unique positive real root x^* if any of the cases 4, 6, 8 hold. For this value of x^*, y^* is given by $y^* = \frac{s(x^*+b)}{h}$. Thus, system (2) has a unique equilibrium point $E^*(x^*, y^*)$.

Example 3.1. *Next, we numerically discuss the existence of the* $E^*(x^*, y^*)$. *The value of the parameters are taken as* $a = 1.4,\ k = 0.01,\ d = 0.8,\ w = 2.29,\ \alpha = 0.09,\ \beta = 0.6,\ s = 0.2,\ h = 0.15,\ b = 0.3$. *For this set of parameter values* $P_4 = 0.000017 > 0,\ P_3 = 0.001519 > 0,\ P_2 = 0.01542 > 0,\ P_1 = 0.062943 > 0,\ P_0 = -0.018367 < 0$, *thus case 4 holds. Four equilibrium points* $E_0(0,0)$, $E_1(1.75,0)$, $E_2(0.0.4)$ *and* $E^*(0.273052, 0.764069)$ *obtained. Therefore, system* (2) *has unique interior equilibrium point* $E^*(0.273052, 0.764069)$ *for the given set of parameter values.*

The Jacobian matrix J of the system (2) is given as

$$J = \begin{pmatrix} \frac{a}{1+ky} - 2dx - \frac{wy}{(1+\alpha x)^2(1+\beta y)} & \frac{-akx}{(1+ky)^2} - \frac{wx}{(1+\alpha x)(1+\beta y)^2} \\ \frac{hy^2}{(b+x)^2} & s - \frac{2hy}{b+x} \end{pmatrix}.$$

The stability conditions of E_0, E_1, E_2 and E^* are discussed in following lemmas:
Lemma 1: Trivial equilibrium $E_0(0,0)$ is always unstable, as both the eigenvalues $\lambda_1 = a$ and $\lambda_2 = s$ of the Jacobian matrix J_{E_0} are always positive, where

$$J_{E_0} = \begin{pmatrix} a & 0 \\ 0 & s \end{pmatrix}. \tag{10}$$

Lemma 2: Predator free axial equilibrium point $E_1(\frac{a}{d}, 0)$ is a saddle point (unstable), as eigenvalues $\lambda_1 = -a < 0$ and $\lambda_2 = s > 0$ of J_{E_1}, where

$$J_{E_1} = \begin{pmatrix} -a & -\frac{ka^2}{d} - \frac{wa}{a\alpha+d} \\ 0 & s \end{pmatrix}. \tag{11}$$

Lemma 3: The Jacobian matrix J_{E_2} of the system (2) around the prey free axial equilibrium $E_2(0, \frac{bs}{h})$ is given by

$$J_{E_2} = \begin{pmatrix} \frac{ah}{h+bsk} - \frac{bsw}{h+bs\beta} & 0 \\ \frac{s^2}{bh} & -s \end{pmatrix}. \tag{12}$$

The eigenvalues $\lambda_1 = \frac{ah}{h+bsk} - \frac{bsw}{h+bs\beta}$ and $\lambda_2 = -s$ of the Jacobian matrix J_{E_2} are negative, provided

$$\frac{ah}{h+bsk} < \frac{bsw}{h+bs\beta}. \tag{13}$$

E_2 is locally asymptotically stable (LAS) if the condition (13) holds and a saddle point otherwise.
Lemma 4: Jacobian matrix J_{E^*} about interior equilibrium point $E^*(x^*, y^*)$ is given by

$$J_{E^*} = \begin{pmatrix} -dx^* + \frac{w\alpha x^* y^*}{(1+\alpha x^*)^2(1+\beta y^*)} & -\frac{akx^*}{(1+ky^*)^2} - \frac{wx^*}{(1+\alpha x^*)(1+\beta y^*)^2} \\ \frac{hy^{*2}}{(b+x^*)^2} & -\frac{hy^*}{(b+x^*)} \end{pmatrix} = \begin{pmatrix} a_{11} & a_{12} \\ a_{21} & a_{22} \end{pmatrix}.$$

The characteristic equation of the Jacobian matrix J_{E^*} is given by

$$\lambda^2 - (a_{11} + a_{22})\lambda + (a_{11}a_{22} - a_{12}a_{21}) = 0. \tag{14}$$

By Routh-Hurwitz criterion, system (2) is LAS around the interior equilibrium point $E^*(x^*, y^*)$ if $-(a_{11} + a_{22}) > 0$ and $(a_{11}a_{22} - a_{12}a_{21}) > 0$.
Straight forward calculations show that $E^*(x^*, y^*)$ is LAS provided condition

$$dx^* > \frac{w\alpha x^* y^*}{(1+\alpha x^*)^2(1+\beta y^*)} \tag{15}$$

holds.

4. Analysis of delayed model system

4.1. Local stability analysis and Hopf-bifurcation

Let $\bar{x} = x - x^*$, $\bar{y} = y - y^*$ be the perturbed variables about $E^*(x^*, y^*)$. Then the linearized form of the system (3) is given by (bar sign is dropped for simplicity)

$$\frac{d}{dt}\begin{pmatrix} x(t) \\ y(t) \end{pmatrix} = A_1 \begin{pmatrix} x(t) \\ y(t) \end{pmatrix} + A_2 \begin{pmatrix} x(t-\tau) \\ y(t-\tau) \end{pmatrix}, \tag{16}$$

where

$$A_1 = \begin{pmatrix} -dx^* + \frac{w\alpha x^* y^*}{(1+\alpha x^*)^2(1+\beta y^*)} & -\frac{akx^*}{(1+ky^*)^2} - \frac{wx^*}{(1+\alpha x^*)(1+\beta y^*)^2} \\ 0 & s \end{pmatrix} = \begin{pmatrix} a_{11} & a_{12} \\ 0 & s \end{pmatrix},$$

$$A_2 = \begin{pmatrix} 0 & 0 \\ \frac{hy^{*2}}{(b+x^*)^2} & -\frac{2hy^*}{(b+x^*)} \end{pmatrix} = \begin{pmatrix} 0 & 0 \\ b_{21} & b_{22} \end{pmatrix}.$$

The characteristic equation of the linearized system (16) is given by

$$\det(A_1 + e^{-\lambda\tau}A_2 - \lambda I_2) = 0, \tag{17}$$

where I_2 is the identity matrix of order 2. In the simplified form, Eq. (17) can be rewritten as

$$\lambda^2 + B_1\lambda + B_0 + e^{-\lambda\tau}(C_1\lambda + C_0) = 0, \tag{18}$$

where $B_1 = -(a_{11} + s)$, $B_0 = a_{11}s$, $C_1 = -b_{22}$, $C_0 = a_{11}b_{22} - a_{12}b_{21}$.
Eq. (18) has a pair of imaginary roots $\pm i\omega$ ($\omega > 0$) if and only if ω satisfies

$$-\omega^2 + B_1 i\omega + B_0 + (\cos\omega\tau - i\sin\omega\tau)(C_1 i\omega + C_0) = 0. \tag{19}$$

Separating the real and imaginary parts, we have

$$\omega^2 - B_0 = C_0\cos\omega\tau + C_1\omega\sin\omega\tau, \tag{20}$$

$$B_1\omega = C_0\sin\omega\tau - C_1\omega\cos\omega\tau. \tag{21}$$

Squaring and adding Eqs. (20) and (21), we get

$$\omega^4 + (B_1^2 - 2B_0 - C_1^2)\omega^2 + (B_0^2 - C_0^2) = 0. \tag{22}$$

Eq. (22) has a unique positive root ω_0, which is given by

$$\omega_0 = \sqrt{\frac{-(B_1^2 - 2B_0 - C_1^2) + \sqrt{(B_1^2 - 2B_0 - C_1^2)^2 - 4(B_0^2 - C_0^2)}}{2}}. \tag{23}$$

Now, for the existence of unique positive root of the equation (22), it is necessary that the values $(B_1^2 - 2B_0 - C_1^2)$ and $(B_0^2 - C_0^2)$ cannot be positive at the same time and also the sign of $(B_0^2 - C_0^2)$ must be negative.
Substituting ω_0, we obtained the corresponding critical value of time delay τ_j as

$$\tau_j = \frac{1}{\omega_0}\left\{\arccos\left(\frac{C_0(\omega_0^2 - B_0) - B_1C_1\omega_0^2}{C_0^2 + C_1^2\omega_0^2}\right) + 2j\pi\right\}, \quad j = 0, 1, 2, \cdots. \tag{24}$$

According to Butler's lemma [42], the interior equilibrium point $E^*(x^*, y^*)$ remains stable for $\tau < \tau_0$, where $\tau_0 = \min\{\tau_j\}$, $j = 0, 1, 2, \cdots$ and $E^*(x^*, y^*)$ becomes unstable when the value of τ exceeds

the critical value τ_0 ($\tau > \tau_0$), provided the transversality condition is satisfied.
Here, we will drive the transversality condition $\left[\frac{d(\mathrm{Re}(\lambda(\tau)))}{d\tau}\right]_{\tau=\tau_0} \neq 0$. For this, we consider, $\lambda(\tau) = \zeta(\tau) + i\omega(\tau)$ be a root of the Eq. (18) such that $\zeta(\tau_0) = 0, \quad \omega(\tau_0) = \omega_0$. Using this substitution in Eq. (18) and taking the derivative with respect to τ, we get

$$\left[\frac{d\lambda}{d\tau}\right]^{-1} = \frac{(2\lambda + B_1)e^{\lambda\tau}}{\lambda(C_1\lambda + C_0)} + \frac{C_1}{\lambda(C_1\lambda + C_0)} - \frac{\tau}{\lambda}. \tag{25}$$

Now

$$\left(\left[\frac{d(\mathrm{Re}(\lambda))}{d\tau}\right]^{-1}\right)_{\lambda=i\omega_0} = \frac{2\omega_0^2 + (B_1^2 - 2B_0 - C_1^2)}{C_1^2\omega_0^2 + C_0^2}, \tag{26}$$

which shows that

$$\left[\frac{d(\mathrm{Re}(\lambda(\tau)))}{d\tau}\right]_{\tau=\tau_0} \neq 0, \quad \text{if} \quad 2\omega_0^2 + (B_1^2 - 2B_0 - C_1^2) \neq 0. \tag{27}$$

Thus, the transversality condition is satisfied. Therefore, Hopf-bifurcation occurs at $\tau = \tau_0$.

Theorem 4.1. *Let us consider that the interior equilibrium point $E^*(x^*, y^*)$ exists and is LAS for a non-delay system* (2).

(i) Then there exists $\tau = \tau_0$ such that the interior equilibrium point $E^*(x^*, y^*)$ of the delay system (3) *remains LAS for $\tau \in [0, \tau_0)$ and becomes unstable for $\tau > \tau_0$.*

(ii) The system (3) *undergoes the Hopf-bifurcation at $\tau = \tau_0$, if the transversality condition holds i.e., $2\omega_0^2 + (B_1^2 - 2B_0 - C_1^2) \neq 0$.*

4.2. Direction and stability of Hopf-bifurcation

In the above discussion, we have observed that at $\tau = \tau_0$, the system (3) undergoes the Hopf-bifurcation under certain condition. That is, a family of periodic solutions bifurcate from the interior equilibrium point E^*. Here, we have analyzed the direction, stability and period of the bifurcating periodic solutions arises through Hopf-bifurcation by using the center manifold theorem and normal form theory given by Hassard et al. [43].

Let $\tau = \tau_0 + \mu$, $\mu \in \mathbb{R}$, so that $\mu = 0$ is a Hopf-bifurcation value for the model system (3). Let us consider the transformation $X_1 = x - x^*$, $X_2 = y - y^*$ and $\mu = \tau - \tau_0$. We normalize the time delay with the scaling $t \to \frac{t}{\tau}$. Now, the system (3) transforms to the following functional differential equation in C ($C = C([-1, 0), \mathbb{R}^2)$ be the space of continuous real-valued functions) as

$$\frac{dX}{dt} = L_\mu(X_t) + f(\mu, X_t), \tag{28}$$

where $X(t) = (X_1(t), X_2(t))^T \in \mathbb{R}^2$, $X_t(\theta) = X(t + \theta)$, $\theta \in [-1, 0]$ and $L_\mu : C \to \mathbb{R}$, $f : \mathbb{R} \times C \to \mathbb{R}$ are given by

$$L_\mu(\phi) = (\tau_0 + \mu)[J_1\phi(0) + J_2\phi(-1)], \tag{29}$$

such that

$$J_1 = \begin{pmatrix} -dx^* + \frac{w\alpha x^* y^*}{(1+\alpha x^*)^2(1+\beta y^*)} & -\frac{akx^*}{(1+ky^*)^2} - \frac{wx^*}{(1+\alpha x^*)(1+\beta y^*)^2} \\ 0 & s \end{pmatrix} = \begin{pmatrix} a_{11} & a_{12} \\ 0 & s \end{pmatrix},$$

$$J_2 = \begin{pmatrix} 0 & 0 \\ \frac{hy^{*2}}{(x^*+b)^2} & -\frac{2hy^*}{(x^*+b)} \end{pmatrix} = \begin{pmatrix} 0 & 0 \\ b_{21} & b_{22} \end{pmatrix},$$

and

$$f(\mu,\phi)=(\tau_0+\mu)\begin{pmatrix} p_1\phi_1^2(0)+p_2\phi_1(0)\phi_2(0)+p_3\phi_2^2(0) \\ p_4\phi_1^2(-1)+p_5\phi_1(-1)\phi_2(-1)+p_6\phi_2^2(-1)\end{pmatrix},$$

where $\phi(\theta)=(\phi_1(\theta),\phi_2(\theta))^T\in C$ and values of $p_i,\ i=1,2,\cdots,6$ are given in Appendix.

By the Reisz representation theorem, $\exists$ a function $\eta(\theta,\mu)$ whose components are of bounded variation for $\theta\in[-1,0]$ such that

$$L_\mu\phi=\int_{-1}^{0}\phi(\theta)d\eta(\theta,\mu) \qquad \text{for } \phi\in C. \tag{30}$$

We choose

$$\eta(\theta,\mu)=(\tau_0+\mu)[J_1\delta(\theta)+J_2\delta(\theta+1)], \tag{31}$$

where $\delta(\theta)$ is the Dirac delta function. For $\phi\in C^1([-1,0],\mathbb{R}^2)$, define

$$A(\mu)\phi=\begin{cases}\frac{d\phi(\theta)}{d\theta}, & \theta\in[-1,0),\\ \int_{-1}^{0}\phi(\sigma)d\eta(\sigma,\mu) & \theta=0,\end{cases}$$

and

$$R(\mu)\phi=\begin{cases}0 & \theta\in[-1,0),\\ f(\theta,\mu) & \theta=0.\end{cases}$$

Now, the system (28) can be written as

$$\dot{X}_t=A(\mu)X_t+R(\mu)X_t, \tag{32}$$

where $X_t(\theta)=X(t+\theta)$ for $\theta\in[-1,0]$. For $\psi\in C^1([0,1],(\mathbb{R}^2)^*)$, define

$$A^*\psi(\sigma)=\begin{cases}-\frac{d\psi(\sigma)}{d\sigma}, & \sigma\in(0,1],\\ \int_{-1}^{0}\psi(-t)d\eta^T(t,0), & \sigma=0,\end{cases}$$

and a bilinear inner product

$$<\psi,\phi>=\bar{\psi}(0)\phi(0)-\int_{\theta=-1}^{0}\int_{\xi=0}^{\theta}\bar{\psi}(\xi-\theta)d\eta(\theta)\phi(\xi)d\xi, \tag{33}$$

where $\eta(\theta)=\eta(\theta,0)$. Denote $A(0)$ by A and A^* are adjoint operators. Since $\pm i\omega_0\tau_0$ are the eigenvalues of A and A^*, respectively. Next, we calculate the eigenvectors of A and A^* corresponding to eigenvalues $+i\omega_0\tau_0$ and $-i\omega_0\tau_0$, respectively. Let $q(\theta)=(\alpha_1,\alpha_2)^Te^{i\omega_0\tau_0\theta}$ be the eigenvector of A corresponding to eigenvalue $+i\omega_0\tau_0$, then

$$Aq(\theta)=i\omega_0\tau_0q(\theta), \tag{34}$$

putting $\theta=0$, we get

$$\tau_0\begin{pmatrix} i\omega_0-a_{11} & -a_{12} \\ -b_{21}e^{-i\omega_0\tau_0} & i\omega_0-s-b_{22}e^{-i\omega_0\tau_0}\end{pmatrix}q(0)=\begin{pmatrix}0\\0\end{pmatrix}.$$

By choosing $\alpha_1=1$, we obtain

$$\alpha_2=\frac{i\omega_0-a_{11}}{a_{12}}.$$

Similarly, let $q^*(\sigma) = N(\alpha_1^*, \alpha_2^*)^T e^{i\omega_0\tau_0\sigma}$ be the eigenvector of A^* corresponding to $-i\omega_0\tau_0$, we have $A^*q^*(\sigma) = -i\omega_0\tau_0 q^*(\sigma)$, where $\alpha_1^* = 1$, $\alpha_2^* = -\frac{(i\omega_0 + a_{11})}{b_{21}e^{-i\omega_0\tau_0}}$.
Now, we select the value of N using the conditions $\langle q^*(s), q(\theta)\rangle = 1$ and $\langle q^*(s), q(\theta)\rangle = 0$.

$$\begin{aligned}
&\langle q^*(s), q(\theta)\rangle \\
&= \bar{N}(1, \bar{\alpha_2^*})(1, \alpha_2)^T - \int_{\theta=-1}^{0}\int_{\xi=0}^{\theta} \bar{N}(1, \bar{\alpha_2^*})e^{-i\omega_0\tau_0(\xi-\theta)}d\eta(\theta) \times (1, \alpha_2)^T e^{i\omega_0\tau_0\xi}d\xi \\
&= \bar{N}\left\{1 + \alpha_2\bar{\alpha_2^*} + \tau_0(b_1 + b_2\alpha_2)\bar{\alpha_2^*}e^{-i\omega_0\tau_0}\right\},
\end{aligned}$$

which gives

$$\bar{N} = \frac{1}{1 + \alpha_2\bar{\alpha_2^*} + \tau_0(b_1 + b_2\alpha_2)\bar{\alpha_2^*}e^{-i\omega_0\tau_0}}.$$

Now, to derive the center manifold C_0 at $\mu = 0$, we need to compute its coordinates. Let, X_t is the solution of Eq. (32) when $\mu = 0$.

Define

$$z(t) = \langle q^*, X_t\rangle, \quad W(t, \theta) = X_t(\theta) - 2Re\{z(t)q(\theta)\}. \tag{35}$$

On the center manifold C_0, we have

$$W(t, \theta) = W(z, \bar{z}, \theta) = W_{20}(\theta)\frac{z^2}{2} + W_{11}(\theta)z\bar{z} + W_{02}(\theta)\frac{\bar{z}^2}{2!} + W_{30}(\theta)\frac{z^3}{3!} + \cdots, \tag{36}$$

where z and $\bar{z}$ are the local coordinates of the center manifold C_0 in the direction of q^* and $\bar{q^*}$. We now consider only the real solution $X_t \in C_0$ of Eq. (32), which gives

$$\begin{aligned}
\dot{z} &= i\omega_0\tau_0 z + \bar{q^*}f(0, W(z, \bar{z}, 0) + 2Re\{zq(\theta)\}) \\
&= i\omega_0\tau_0 z + g(z, \bar{z}),
\end{aligned} \tag{37}$$

where

$$\begin{aligned}
g(z, \bar{z}) &= \bar{q^*}(0)f_0(z, \bar{z}) \\
&= g_{20}\frac{z^2}{2} + g_{11}z\bar{z} + g_{02}\frac{\bar{z}^2}{2} + g_{21}\frac{z^2\bar{z}}{2} + \cdots.
\end{aligned} \tag{38}$$

From Eqs. (35) and (36) we have

$$\begin{aligned}
X_t(\theta) &= W(z, \bar{z}, \theta) + 2Re\{zq(\theta)\} \\
&= W_{20}(\theta)\frac{z^2}{2} + W_{11}(\theta)z\bar{z} + W_{02}(\theta)\frac{\bar{z}^2}{2} + z(1, \alpha_2)^T e^{i\omega_0\tau_0\theta} \\
&\quad + \bar{z}(1, \bar{\alpha}_2)^T e^{-i\omega_0\tau_0\theta} + \cdots,
\end{aligned} \tag{39}$$

so that

$$\begin{aligned}
X_{1t}(0) &= z + \bar{z} + W_{20}^1(0)\frac{z^2}{2} + W_{11}^1(0)z\bar{z} + W_{02}^1(0)\frac{\bar{z}^2}{2} + \cdots, \\
X_{2t}(0) &= \alpha_2 z + \bar{\alpha}_2\bar{z} + W_{20}^2(0)\frac{z^2}{2} + W_{11}^2(0)z\bar{z} + W_{02}^2(0)\frac{\bar{z}^2}{2} + \cdots, \\
X_{1t}(-1) &= ze^{-i\omega_0\tau_0} + \bar{z}e^{i\omega_0\tau_0} + W_{20}^1(-1)\frac{z^2}{2} + W_{11}^1(-1)z\bar{z} + W_{02}^1(-1)\frac{\bar{z}^2}{2} + \cdots, \\
X_{2t}(-1) &= \alpha_2 ze^{-i\omega_0\tau_0} + \bar{\alpha}_2\bar{z}e^{i\omega_0\tau_0} + W_{20}^2(-1)\frac{z^2}{2} + W_{11}^2(-1)z\bar{z} + W_{02}^2(-1)\frac{\bar{z}^2}{2} + \cdots.
\end{aligned}$$

$$
\begin{aligned}
g(z,\bar{z}) &= \tau_0\bar{N}(1,\bar{\alpha_2^*}) \times f_0(z,\bar{z}) \\
&= \tau_0\bar{N}(1,\bar{\alpha_2^*}) \begin{pmatrix} p_1X_{1t}^2(0) + p_2X_{1t}(0)X_{2t}(0) + p_3X_{2t}^2(0) \\ p_4X_{1t}^2(-1) + p_5X_{1t}(-1)X_{2t}(-1) + p_6X_{2t}^2(-1) \end{pmatrix} \\
&= \tau_0\bar{N}\left[z^2\left\{p_1 + p_2\alpha_2 + p_3\alpha_2^2 + e^{-2i\omega_0\tau_0}\bar{\alpha_2^*}(p_4 + p_5\alpha_2 + p_6\alpha_2^2)\right\} + z\bar{z}\left\{2p_1\right.\right. \\
&\quad +2p_2\mathrm{Re}(\alpha_2) + 2p_3\bar{\alpha}_2\alpha_2 + 2p_4\bar{\alpha_2^*} + 2p_5\bar{\alpha_2^*}\mathrm{Re}(\alpha_2) + 2p_6\bar{\alpha_2^*}\bar{\alpha}_2\alpha_2\Big\} \\
&\quad +\bar{z}^2\left\{p_1 + p_2\bar{\alpha}_2 + p_3\bar{\alpha}_2^2 + e^{2i\omega_0\tau_0}\bar{\alpha_2^*}(p_4 + p_5\bar{\alpha}_2 + p_6\bar{\alpha}_2^2)\right\} \\
&\quad +z^2\bar{z}\left\{p_1W_{20}^1(0) + \frac{1}{2}p_2\bar{\alpha}_2W_{20}^1(0) + 2p_1W_{11}^1(0) + \frac{1}{2}p_2W_{20}^2(0)\right. \\
&\quad +p_3\bar{\alpha}_2W_{20}^2(0) + p_2W_{11}^2(0) + p_2W_{11}^1(0)\alpha_2 + 2p_3W_{11}^2(0)\alpha_2 \\
&\quad +e^{i\omega_0\tau_0}\bar{\alpha_2^*}\left(p_4W_{20}^1(-1) + \frac{1}{2}p_5\bar{\alpha}_2W_{20}^1(-1) + \frac{1}{2}p_5W_{20}^2(-1)\right. \\
&\quad \left.+p_6\bar{\alpha}_2W_{20}^2(-1)\right) + e^{-i\omega_0\tau_0}\bar{\alpha_2^*}\left(2p_4W_{11}^1(-1) + p_5W_{11}^2(-1)\right. \\
&\quad \left.\left.\left.+p_5W_{11}^1(-1)\alpha_2 + 2p_6W_{11}^2(-1)\alpha_2\right)\right\}\right].
\end{aligned}
$$

Comparing the coefficient with (38), we have

$$
\begin{aligned}
g_{20} =& 2\tau_0\bar{N}\left\{p_1 + p_2\alpha_2 + p_3\alpha_2^2 + e^{-2i\omega_0\tau_0}\bar{\alpha_2^*}(p_4 + p_5\alpha_2 + p_6\alpha_2^2)\right\}, \\
g_{11} =& \tau_0\bar{N}\left\{2p_1 + 2p_2\mathrm{Re}(\alpha_2) + 2p_3\bar{\alpha}_2\alpha_2 + 2p_4\bar{\alpha_2^*} + 2p_5\bar{\alpha_2^*}\mathrm{Re}(\alpha_2) + 2p_6\bar{\alpha_2^*}\bar{\alpha}_2\alpha_2\right\}, \\
g_{02} =& 2\tau_0\bar{N}\left\{p_1 + p_2\bar{\alpha}_2 + p_3\bar{\alpha}_2^2 + e^{2i\omega_0\tau_0}\bar{\alpha_2^*}(p_4 + p_5\bar{\alpha}_2 + p_6\bar{\alpha}_2^2)\right\}, \\
g_{21} =& \left\{p_1W_{20}^1(0) + \frac{1}{2}p_2\bar{\alpha}_2W_{20}^1(0) + 2p_1W_{11}^1(0) + \frac{1}{2}p_2W_{20}^2(0) + p_3\bar{\alpha}_2W_{20}^2(0)\right. \\
&+p_2W_{11}^2(0) + p_2W_{11}^1(0)\alpha_2 + 2p_3W_{11}^2(0)\alpha_2 \\
&+e^{i\omega_0\tau_0}\bar{\alpha_2^*}\left(p_4W_{20}^1(-1) + \frac{1}{2}p_5\bar{\alpha}_2W_{20}^1(-1) + \frac{1}{2}p_5W_{20}^2(-1) + p_6\bar{\alpha}_2W_{20}^2(-1)\right) \\
&\left.+e^{-i\omega_0\tau_0}\bar{\alpha_2^*}\left(2p_4W_{11}^1(-1) + p_5W_{11}^2(-1) + p_5W_{11}^1(-1)\alpha_2 + 2p_6W_{11}^2(-1)\alpha_2\right)\right\}.
\end{aligned} \tag{40}
$$

The expression of g_{21} depends on the values of $W_{20}^i(\theta)$ and $W_{11}^i(\theta)$, where $i = 1, 2$. Therefore, we need to compute these values.
From Eqs. (35) and (37), we have

$$
\begin{aligned}
\dot{W} &= \dot{X}_t - \dot{z}q - \dot{\bar{z}}\bar{q} \\
&= \begin{cases} AW - 2Re\{\bar{q}^*(0)f_0q(\theta)\}, & \theta \in [-1, 0), \\ AW - 2Re\{\bar{q}^*(0)f_0q(\theta)\} + f_0, & \theta = 0, \end{cases} \qquad (41) \\
&= AW + H(z,\bar{z},\theta) \qquad (42)
\end{aligned}
$$

with

$$
H(z,\bar{z},\theta) = H_{20}(\theta)\frac{z^2}{2} + H_{11}(\theta)z\bar{z} + H_{02}(\theta)\frac{\bar{z}^2}{2} + \cdots. \tag{43}
$$

Also on C_0, using the chain rule, we get

$$
\dot{W} = W_z\dot{z} + W_{\bar{z}}\dot{\bar{z}}. \tag{44}
$$

It follows from Eqs. (38), (42) and (44)

$$(A - 2i\omega_0\tau_0)W_{20} = -H_{20}, \tag{45}$$
$$AW_{11} = -H_{11}. \tag{46}$$

Now, for $\theta \in [-1, 0)$, we have

$$\begin{aligned} H(z,\bar{z},\theta) &= -2Re\{\bar{q^*}(0)f_0q(\theta)\} \\ &= -\bar{q^*}(0)f_0q(\theta) - q^*(0)\bar{f}_0\bar{q}(\theta) \\ &= -g(z,\bar{z})q(\theta) - \bar{g}(z,\bar{z})\bar{q}(\theta) \\ &= -\left(g_{20}q(\theta) + \bar{g}_{02}\bar{q}(\theta)\right)\frac{z^2}{2} - \left(g_{11}q(\theta) + \bar{g}_{11}\bar{q}(\theta)\right)z\bar{z} + \cdots, \end{aligned} \tag{47}$$

which on comparing the coefficients with Eq. (43) gives

$$H_{20}(\theta) = -\left(g_{20}q(\theta) + \bar{g}_{02}\bar{q}(\theta)\right), \tag{48}$$
$$H_{11}(\theta) = -\left(g_{11}q(\theta) + \bar{g}_{11}\bar{q}(\theta)\right). \tag{49}$$

From Eqs. (45), (48) and the definition of A, we have

$$\dot{W}_{20}(\theta) = 2i\omega_0\tau_0W_{20}(\theta) + g_{20}q(\theta) + \bar{g}_{02}\bar{q}(\theta), \tag{50}$$

Note that $q(\theta) = q(0)e^{i\omega_0\tau_0\theta}$, we have

$$W_{20}(\theta) = \frac{ig_{20}}{\omega_0\tau_0}q(\theta) + \frac{i\bar{g}_{02}}{3\omega_0\tau_0}\bar{q}(\theta) + E_1e^{2i\omega_0\tau_0\theta}. \tag{51}$$

Similarly from (46), (49) and using the definition of A, we have

$$\begin{aligned} \dot{W}_{11}(\theta) &= g_{11}q(\theta) + \bar{g}_{11}\bar{q}(\theta), \\ W_{11}(\theta) &= -\frac{ig_{11}}{\omega_0\tau_0}q(\theta) + \frac{i\bar{g}_{11}}{\omega_0\tau_0}\bar{q}(\theta) + E_2, \end{aligned} \tag{52}$$

where $E_1 = (E_1^{(1)}, E_1^{(2)})$, $E_2 = (E_2^{(1)}, E_2^{(2)}) \in \mathbb{R}^2$ are constant vectors. Next, we will determine the values of E_1 and E_2, which is given in Appendix.
Thus, we can obtain $W_{20}(\theta)$ and $W_{11}(\theta)$ from Eqs. (51) and (52). Also, g_{21} in Eq. (41) can be expressed in terms of parameters and delay. Now, we calculate to followings values:

$$\begin{aligned} C_1(0) &= \frac{i}{2\omega_0\tau_0}\left(g_{20}g_{11} - 2|g_{11}|^2 - \frac{|g_{02}|^2}{3}\right) + \frac{g_{21}}{2}, \\ \mu_2 &= -\frac{\mathrm{Re}\{C_1(0)\}}{\mathrm{Re}\{\lambda'(\tau_0)\}}, \\ \beta_2 &= 2\mathrm{Re}\{C_1(0)\}, \\ T_2 &= -\frac{\mathrm{Im}\{C_1(0)\} + \mu_2\mathrm{Im}\{\lambda'(\tau_0)\}}{\omega_0\tau_0}, \end{aligned} \tag{53}$$

which determines the properties of bifurcating periodic solutions in the center manifold at the critical value τ_0.

Theorem 4.2. *The sign of μ_2, β_2 and T_2 determine the direction of Hopf-bifurcation, stability of the bifurcating periodic solutions and the period of the bifurcating periodic solutions respectively. If $\mu_2 > 0$ (< 0), then the Hopf-bifurcation is supercritical (subcritical) and the bifurcating periodic solutions exist for $\tau > \tau_0$ ($\tau < \tau_0$). The bifurcating periodic solutions are stable if $\beta_2 < 0$ and are unstable if $\beta_2 > 0$. Furthermore, the period of the bifurcating periodic solutions increases if $T_2 > 0$ and decreases if $T_2 < 0$.*

5. Spatially explicit model system

In this section, we have incorporated the spatial component of ecological interactions into the temporal system (2) by extending the ODEs system to PDEs system using the reaction-diffusion equations. At any position $(U, V) \in \Omega$ and time t, the population densities of prey and predator are given by $x(t, U, V)$ and $y(t, U, V)$, respectively, where $\Omega \subset \mathbb{R}^2$ is a bounded domain with smooth boundary $\partial\Omega$. Then the spatiotemporal model corresponding to the temporal model (2) is given by the following reaction-diffusion system:

$$\begin{aligned} \frac{\partial x}{\partial t} &= \frac{ax}{1+ky} - dx^2 - \frac{wxy}{(1+\alpha x)(1+\beta y)} + d_1\Delta x, \\ \frac{\partial y}{\partial t} &= sy - \frac{hy^2}{x+b} + d_2\Delta y, \end{aligned} \tag{54}$$

subjected to non-negative initial conditions and zero-flux boundary conditions

$$\begin{aligned} &x(0, U, V) \geq 0, \quad y(0, U, V) \geq 0, \quad (U, V) \in \Omega, \\ &\frac{\partial x}{\partial \nu} = \frac{\partial y}{\partial \nu} = 0, \quad (U, V) \in \partial\Omega, \quad t > 0, \end{aligned} \tag{55}$$

where d_1 and d_2 are self-diffusion coefficients of prey and predator respectively, ν is the outward unit normal to $\partial\Omega$ and the Laplace operator $\Delta = \frac{\partial^2}{\partial U^2} + \frac{\partial^2}{\partial V^2}$.

In the above model formulation (54), we have taken care of only the self-diffusion terms [23, 24]. However, in realistic ecological framework, the movement of prey individuals is highly influenced by the presence, absence, abundance and scarcity of predator population and vice-versa. This phenomenon is termed as cross-diffusion [32, 33, 34] and it cannot be captured in spatiotemporal predator-prey model with self-diffusion terms only. Very few works [39, 40] have been done taking cross-diffusion along with self-diffusion in predator-prey model with the fear effect. Now, including the cross-diffusion terms, the system (54) takes the following form:

$$\begin{aligned} \frac{\partial x}{\partial t} &= \frac{ax}{1+ky} - dx^2 - \frac{wxy}{(1+\alpha x)(1+\beta y)} + \Delta(d_1 x + d_{12} xy), \\ \frac{\partial y}{\partial t} &= sy - \frac{hy^2}{x+b} + \Delta(d_2 y + d_{21} xy), \end{aligned} \tag{56}$$

where d_{12} and d_{21} are cross-diffusion coefficients of prey and predator populations, respectively. We have assumed that both d_{12} and d_{21} are positive constants. $d_{12} > 0$ implies that prey is moving towards the lower concentration of predators and $d_{21} > 0$ signifies that predator species prefer to hunt prey from the lower groups of prey population to avoid the group defense by larger groups. We take the same initial and boundary conditions as given in Eq. (55).

5.1. Stability analysis of the spatial model system

In order to discuss the linear stability analysis of the model system (56) about the spatially homogeneous steady state $E^*(x^*, y^*)$, we linearize this system using the transformations

$$\begin{aligned} x(t, U, V) &= x^* + \hat{x}(t, U, V), \\ y(t, U, V) &= y^* + \hat{y}(t, U, V), \end{aligned} \tag{57}$$

where $\hat{x}(t, U, V)$ and $\hat{y}(t, U, V)$ are small time and space perturbations. Conventionally, $\hat{x}$ and $\hat{y}$ are taken as

$$\begin{aligned} \hat{x}(t, U, V) &= \epsilon_1 \exp\left(\lambda_K t + i(K_U U + K_V V)\right), \\ \hat{y}(t, U, V) &= \epsilon_2 \exp\left(\lambda_K t + i(K_U U + K_V V)\right), \end{aligned} \tag{58}$$

where $0 < \epsilon_1,\ \epsilon_2 \ll 1$ and λ_K is the wavelength. Also, $\mathtt{K} = (K_U, K_V)$ is the wave number vector and $K = |\mathtt{K}|$ is the wave number.
Substituting (57) and (58) in the spatial system (56), we have

$$\begin{aligned} \frac{\partial \hat{x}}{\partial t} &= a_{11}\hat{x} + a_{12}\hat{y} - K^2(d_1 + d_{12}y^*)\hat{x} - K^2(d_{12}x^*)\hat{y}, \\ \frac{\partial \hat{y}}{\partial t} &= a_{21}\hat{x} + a_{22}\hat{y} - K^2(d_{21}y^*)\hat{x} - K^2(d_2 + d_{21}x^*)\hat{y}, \end{aligned} \tag{59}$$

where
$a_{11} = -dx^* + \frac{w\alpha x^* y^*}{(1+\alpha x^*)^2(1+\beta y^*)},\ a_{12} = -\frac{akx^*}{(1+ky^*)^2} - \frac{wx^*}{(1+\alpha x^*)(1+\beta y^*)^2},$
$a_{21} = \frac{hy^{*2}}{(b+x^*)^2},\ a_{22} = -\frac{hy^*}{(b+x^*)}.$
The characteristic equation of the linearized system (59) is given by

$$\det(J_K - \lambda I_2) = 0, \tag{60}$$

where

$$J_K = \begin{pmatrix} a_{11} - (d_1 + d_{12}y^*)K^2 & a_{12} - d_{12}x^*K^2 \\ a_{21} - d_{21}y^*K^2 & a_{22} - (d_2 + d_{21}x^*)K^2 \end{pmatrix}.$$

In simplified form, the characteristic Eq. (60) can be rewritten as

$$\lambda^2 + g(K^2)\lambda + h(K^2) = 0, \tag{61}$$

where

$$\begin{aligned} g(K^2) &= -(a_{11} + a_{22}) + K^2(d_1 + d_{12}y^* + d_2 + d_{21}x^*), \\ h(K^2) &= q_1K^4 + q_2K^2 + q_3, \\ q_1 &= d_1d_2 + d_2d_{12}y^* + d_1d_{21}x^* > 0, \\ q_2 &= a_{12}d_{21}y^* + a_{21}d_{12}x^* - a_{22}(d_1 + d_{12}y^*) - a_{11}(d_2 + d_{21}x^*), \\ q_3 &= a_{11}a_{22} - a_{12}a_{21}. \end{aligned}$$

Eq. (61) yield the following dispersion relation

$$2\lambda(K^2) = -g(K^2) \pm \sqrt{(g(K^2))^2 - 4h(K^2)}. \tag{62}$$

According to Routh-Hurwitz criterion for stability $\mathrm{Re}(\lambda) < 0$ if and only if

$$g(K^2) > 0 \ \text{ and } \ h(K^2) > 0. \tag{63}$$

Theorem 5.1. *Suppose that the interior equilibrium point $E^*(x^*, y^*)$ is LAS for the temporal system. Then $E^*(x^*, y^*)$ is LAS for the spatiotemporal system* (56) *iff the condition* (63) *holds.*

5.2. Turing instability

If the homogeneous equilibrium $E^*(x^*, y^*)$ is linearly stable in the absence of diffusion and becomes unstable in the presence of diffusion then these instabilities are called Turing instability. i.e.,

$$\mathrm{Re}(\lambda(K^2 \neq 0)) > 0 \ \text{ for some } K \neq 0 \ \text{ and } \ \mathrm{Re}(\lambda(K^2 = 0)) < 0. \tag{64}$$

Therefore, for this instability to occurs in the spatial system (56), it is necessary that the condition (63) fails to exist. $g(K^2) > 0$ for all $K \neq 0$, as diffusion coefficients are positive and $-(a_{11} + a_{22}) > 0$ from the stability of homogeneous steady state E^*. Thus, for diffusive instability we require that $h(K^2) < 0$ for some $K \neq 0$. Since $h(K^2)$ is a quadratic function of K^2, therefore for $h(K^2)$ to

be negative for some $K \neq 0$, its minimum must be negative. The minimum of $h(K^2)$ reached at $K^2 = K_{cr}^2 = \frac{-q_2}{2q_1}$.
We required

$$\begin{aligned} q_2 =& \frac{hy^*}{(b+x^*)}d_1 + \left(dx^* - \frac{w\alpha x^* y^*}{(1+\alpha x^*)^2(1+\beta y^*)}\right)d_2 + \frac{hy^{*2}(b+2x^*)}{(b+x^*)^2}d_{12} \\ &+ \left(dx^{*2} - \frac{akx^* y^*}{(1+ky^*)^2} - \frac{wx^* y^*(1+2\alpha x^* + \alpha\beta x^* y^*)}{(1+\alpha x^*)^2(1+\beta y^*)^2}\right)d_{21} < 0. \end{aligned} \tag{65}$$

for feasible Turing threshold since K_{cr} is a real number. Also, $h(K_{cr}^2) < 0$ provided

$$\begin{aligned} &(a_{12}d_{21}y^* + a_{21}d_{12}x^* - a_{22}(d_1 + d_{12}y^*) - a_{11}(d_2 + d_{21}x^*))^2 \\ &- 4(d_1d_2 + d_2d_{12}y^* + d_1d_{21}x^*)(a_{11}a_{22} - a_{12}a_{21}) > 0. \end{aligned} \tag{66}$$

i.e.,

$$\begin{aligned} &\left(\frac{hy^*}{(b+x^*)}d_1 + \left(dx^* - \frac{w\alpha x^* y^*}{(1+\alpha x^*)^2(1+\beta y^*)}\right)d_2 + \frac{hy^{*2}(b+2x^*)}{(b+x^*)^2}d_{12} + \left(dx^{*2} - \frac{akx^* y^*}{(1+ky^*)^2}\right.\right. \\ &\left.\left. - \frac{wx^* y^*(1+2\alpha x^* + \alpha\beta x^* y^*)}{(1+\alpha x^*)^2(1+\beta y^*)^2}\right)d_{21}\right)^2 - 4(d_1d_2 + d_2d_{12}y^* + d_1d_{21}x^*)\det(J_{E^*}) > 0. \end{aligned} \tag{67}$$

Theorem 5.2. *The necessary conditions for the occurrence of Turing instability of the system* (56) *around* $E^*(x^*, y^*)$ *are the followings:*

$$\begin{cases} dx^* > \frac{w\alpha x^* y^*}{(1+\alpha x^*)^2(1+\beta y^*)}, \\ \frac{hy^* d_1}{(b+x^*)} + \left(dx^* - \frac{w\alpha x^* y^*}{(1+\alpha x^*)^2(1+\beta y^*)}\right)d_2 + \frac{hy^{*2}(b+2x^*)d_{12}}{(b+x^*)^2} + \left(dx^{*2} - \frac{akx^* y^*}{(1+ky^*)^2}\right. \\ \left. - \frac{wx^* y^*(1+2\alpha x^* + \alpha\beta x^* y^*)}{(1+\alpha x^*)^2(1+\beta y^*)^2}\right)d_{21} < 0 \\ \left(\frac{w\alpha x^* y^*}{(1+\alpha x^*)^2(1+\beta y^*)}\right)d_2 + \left(\frac{akx^* y^*}{(1+ky^*)^2} + \frac{wx^* y^*(1+2\alpha x^* + \alpha\beta x^* y^*)}{(1+\alpha x^*)^2(1+\beta y^*)^2}\right)d_{21} \\ \quad > \frac{hy^*}{(b+x^*)}d_1 + dx^* d_2 + \frac{hy^{*2}(b+2x^*)}{(b+x^*)^2}d_{12} + dx^{*2}d_{21} + 2\sqrt{(d_1d_2 + d_2d_{12}y^* + d_1d_{21}x^*)det(J_{E^*})}. \end{cases} \tag{68}$$

We have considered d_{21} as bifurcation parameter, whose critical value $d_{21} = d_{21}^{cr}$ can be obtained numerically by solving the condition $h(K_{cr}^2) = 0$. The explicit expression of d_{21}^{cr} is obtained as

$$\begin{aligned} d_{21}^{cr} = &\frac{1}{(a_{11}^2x^{*2} - 2a_{11}a_{12}x^*y^* + a_{12}^2y^{*2})}\left(a_{11}a_{22}d_1x^* - 2a_{12}a_{21}d_1x^* - a_{11}^2d_2x^*\right. \\ &+a_{11}a_{21}d_{12}x^{*2} + a_{12}a_{22}d_1y^* + a_{11}a_{12}d_2y^* - a_{12}a_{21}d_{12}x^*y^* - a_{11}a_{22}d_{12}x^*y^* \\ &+a_{12}a_{22}d_{12}y^{*2} + \left(\left(2a_{12}a_{21}d_1x^* - a_{11}a_{22}d_1x^* + a_{11}^2d_2x^* - a_{11}a_{21}d_{12}x^{*2}\right.\right. \\ &\left.\left.-a_{12}a_{22}d_1y^* - a_{11}a_{12}d_2y^* + a_{12}a_{21}d_{12}x^*y^* + a_{11}a_{22}d_{12}x^*y^* - a_{12}a_{22}d_{12}y^{*2}\right)^2 \\ &-(a_{11}^2x^{*2} - 2a_{11}a_{12}x^*y^* + a_{12}^2y^{*2})(a_{22}^2d_1^2 + 4a_{12}a_{21}d_1d_2 - 2a_{11}a_{22}d_1d_2 + a_{11}^2d_2^2 \\ &-2a_{21}a_{22}d_1d_{12}x^* - 2a_{11}a_{21}d_{12}d_2x^* + a_{21}^2d_{12}^2x^{*2} + 2a_{22}^2d_1d_{12}y^* + 4a_{12}a_{21}d_{12}d_2y^* \\ &\left.-2a_{11}a_{22}d_{12}d_2y^* - 2a_{21}a_{22}d_{12}^2x^*y^* + a_{22}^2d_{12}^2y^{*2}))^{\frac{1}{2}}\right). \end{aligned} \tag{69}$$

Turing instability conditions in term of cross-diffusion coefficient d_{21} are summarized in the proposition below.

Proposition 1. *The homogeneous equilibrium $E^*(x^*, y^*)$ remains stable for small amplitude heterogeneous perturbations if $-(a_{11}+a_{22})>0$, $a_{11}a_{22}-a_{12}a_{21}>0$ and $d_{21}<d_{21}^{cr}$ and becomes unstable if $-(a_{11}+a_{22})>0$, $a_{11}a_{22}-a_{12}a_{21}>0$ and $d_{21}>d_{21}^{cr}$.*

Example 5.1. *In this example, we have explored the above phenomenon numerically. Parameter values are taken as*

$$\begin{aligned} &a=1.4,\ k=0.01,\ d=0.8,\ w=2.29,\ \alpha=0.09,\ \beta=0.6,\ s=0.2,\\ &h=0.15,\ b=0.3,\ \ d_1=1,\ \ d_{12}=1,\ \ d_2=1. \end{aligned} \tag{70}$$

The critical value of d_{21} is obtained as $d_{21}^{cr}=12.782416897982463$. At this value $dx^*=0.218442>\frac{w\alpha x^*y^*}{(1+\alpha x^*)^2(1+\beta y^*)}=0.0280853$, $d_1d_2+d_1d_{21}^{cr}x^*+d_{12}d_2y^*=5.25433>0$, $\frac{hy^*d_1}{(b+x^*)}+\left(dx^*-\frac{w\alpha x^*y^*}{(1+\alpha x^*)^2(1+\beta y^*)}\right)d_2+\frac{hy^{*2}(b+2x^*)d_{12}}{(b+x^*)^2}+\left(dx^{*2}-\frac{akx^*y^*}{(1+ky^*)^2}-\frac{wx^*y^*(1+2\alpha x^*+\alpha\beta x^*y^*)}{(1+\alpha x^*)^2(1+\beta y^*)^2}\right)d_{21}=-1.55863<0$ and $\left(\frac{w\alpha x^*y^*}{(1+\alpha x^*)^2(1+\beta y^*)}\right)d_2+\left(\frac{akx^*y^*}{(1+ky^*)^2}+\frac{wx^*y^*(1+2\alpha x^*+\alpha\beta x^*y^*)}{(1+\alpha x^*)^2(1+\beta y^*)^2}\right)d_{21}=2.96512=\frac{hy^*}{(b+x^*)}d_1+dx^*d_2+\frac{hy^{*2}(b+2x^*)}{(b+x^*)^2}d_{12}+dx^{*2}d_{21}+2\sqrt{(d_1d_2+d_2d_{12}y^*+d_1d_{21}x^*)det(J_{E^*})}$. We have shown $Re(\lambda(K^2))$ vs. K plot and $h(K^2)$ vs. K plot for $d_{21}=11,\ 12.782417$ and 13.5 (cf. Figs. 2(a) and 2(b)). When $d_{21}=11<d_{21}^{cr}$, $Re(\lambda(K^2))<0$ and $h(K^2)>0$ for all $K\neq 0$, thus stable homogeneous steady state $E^*(x^*,y^*)=(0.273052,0.764069)$ of the system (56) remains stable. When $d_{21}=13.5>d_{21}^{cr}$, $Re(\lambda(K^2))>0$ and $h(K^2)<0$ for some $K\neq 0$. Thus, cross-diffusion-driven instability occurs for $d_{21}=13.5>d_{21}^{cr}$.

Example 5.2. *In this example, we have illustrated the effect of fear on the cross-diffusion induced instability. For this, we have taken $d_{21}=12.8>d_{21}^{cr}$ form the instability region and other parameters are same as given in Example 5.1, except the level of fear k. At $k=0.3$, $Re(\lambda(K^2))>0$ and $h(K^2)<0$ for some values of $K\neq 0$ i.e., system remains unstable (cf. Figs. 3(a) and 3(b)). Increasing the value of k to 0.5 and 1, it is observed that at $k=1$, $Re(\lambda(K^2))<0$ and $h(K^2)>0$ for all K i.e., system becomes stable (cf. Figs. 3(a) and Figs. 3(b)). Thus, increasing the value of k, cross-diffusive induced instabilities goes to stable dynamics. Thus, level of fear k has a stabilizing effect on the spatial dynamics of the system (56).*

Again, we have plotted $\lambda(K^2))$ vs. K and $h(K^2)$ vs. K plots for three different level of fear $k=0.001,\ 0.05,\ 0.1$ (cf. Figs. 3(c) and 3(d)). Initially at $k=0.001$, $Re(\lambda(K^2))<0$ and $h(K^2)>0$ for all values of K, i.e., system (56) is stable . Increasing the value of k to 0.05 and 0.1, $Re(\lambda(K^2))>0$ and $h(K^2)<0$ for some values of K (cf. Figs. 3(c) and 3(d)) i.e., system is unstable. This implies that stable dynamics of system goes to diffusive instability state with increase in the level of fear k. Therefore, level of fear k has a destabilizing effect on the spatial dynamics of the system (56).

From numerical experiment, we have obtained that $k=k_{cr}=0.22$ is the critical value of k. For $k>k_{cr}$, increasing value of k has stabilizing effect and for $k<k_{cr}$, increasing value of k has destabilizing effect.

Remark 1. *In our previous works with self-diffusion [24] and linear cross-diffusion [39], we have shown that fear level k has stabilizing impact on the spatial dynamics. Whereas, here with nonlinear cross-diffusion, we have found that fear level k has both stabilizing and destabilizing impact on the spatial dynamics.*

6. Numerical simulations

6.1. Simulation results for the temporal system

In this subsection, we have performed the numerical simulations to better understand the system dynamics. Simulation experiments are carried out using the Matlab (R2013a) and Matcont toolbox

for the parameter values

$$a = 1.4,\ k = 0.01,\ d = 0.8,\ w = 2.29,\ \alpha = 0.09,\ \beta = 0.6,\ s = 0.2,\ h = 0.15,\ b = 0.3, \tag{71}$$

at which the model system (2) exhibits the stable dynamics (cf. Figs. 4(a) and 4(b)).

Next, we change the values of α (handling time of prey by the predators) and β (value of mutual interference among the predators) to $\alpha = 2.4$ and $\beta = 0.002$, other parameters remain unaltered. Now, the system (2) is unstable showing the periodic oscillations (cf. Figs. 5(a) and 5(b)). In Fig. 6(a), we have presented the bifurcation diagram of the system (2) taking k as control parameter. In Figs. 6(b) and 6(c), we have shown the prey and predator population densities with change in the value of fear level k. It is observed that oscillatory dynamics settle down to stable state via supercritical Hopf-bifurcation as first Lyapunov coefficient $=-6.750548e^{-1} < 0$. Also, the population density of prey x and predator y is decreasing with increase in fear level k.

Remark 2. *Periodic oscillations of the system* (2) *goes to stable dynamics with increase in fear level k. Thus, fear level k has a stabilizing effect on the temporal dynamics. Also, population densities of prey and predator decreases with an increase in the value of level of fear k. Biologically, as level of fear k increases, it stimulates the costly defensive strategies in prey which ultimately cost its production. As prey is the most favourite food of predator so predator population density also decreases correspondingly.*

6.2. Simulation results for the delay system

System (3) exhibits the stable dynamics around the interior equilibrium $E^*(0.273052, 0.764069)$ in the absence of delay (cf. Figs. 4(a) and 4(b)). Now, we will investigate the effect of gestation delay τ and fear level k on the dynamics of delayed system (3). In the analysis section, we have shown that delayed model (3) undergoes Hopf-bifurcation at $\tau = \tau_0 = 1.89157$, calculated using the formula given in Section 4. We have presented the time series and phase portrait taking $\tau = 1.82 < \tau_0$ and $\tau = 1.94 > \tau_0$ (cf. Figs. 7(a),(b) and 7(c),(d)). Figs. 7(a) and 7(b) show that the system (3) is stable for $\tau = 1.82 < \tau_0 = 1.89157$ and becomes unstable (shows limit cycles) for $\tau = 1.94 > \tau_0 = 1.89157$ (cf. Figs. 7(c) and (7)(d)). The transversality condition $\left[\frac{d(\mathrm{Re}(\lambda(\tau)))}{d\tau}\right]_{\tau=\tau_0=1.89157} = 0.178004 \neq 0$ is satisfied. Next, we have plotted the bifurcation diagram with respect to gestation delay τ in the interval $\tau \in [1.5, 2.25]$ (cf. Fig. 8). It is found that if the gestation delay τ increases gradually, then the interior equilibrium E^* loses its stability at $\tau = \tau_0 = 1.89157$ and system experiences the Hopf-bifurcation.

The formulae to determine the direction, stability, and period of bifurcating period solutions arises through Hopf-bifurcation at $\tau = \tau_0 = 1.89157$ are derived in the analysis section. Here, we have numerically calculated these values as $C_1(0) = -8.2875 - 6.82186i$, $\mu_2 = 46.5579 > 0$, $\beta_2 = -16.575 < 0$ and $T_2 = 8.13517 > 0$, at $\tau_0 = 1.89157$. $\mu_2 = 46.5579 > 0$, implies that Hopf-bifurcation is supercritical. $\beta_2 < 0$, ensues the stability of limit cycles arising through Hopf-bifurcation and their period increases as $T_2 = 8.13517 > 0$. In Fig. 9, we have shown the two solution trajectories of the system (3) starting with different initial conditions. It is observed that they are converging to the same limit cycle, which indicates that the bifurcating periodic solutions are stable for $\tau = 1.94 > \tau_0$.

Next, to illustrate the effect of fear on the delay system (3), we have plotted the bifurcation diagrams taking level of fear (k) as control parameter (cf. Figs. 10(a) and 10(b)). Other parameter values are same as given in (71) with time delay $\tau = 1.98 > \tau_0$. We have observes that the oscillatory behaviour of the system (3) is settled down to the stable dynamics with increase in the value of fear level (k). Time series and phase diagrams are also plotted taking fear level $k = 0.5$ and $k = 0.7$ (Figs. 11(a) and 11(b)). At $k = 0.5$, $\tau = 1.98 > \tau_0$, system (3) exhibits a limit cycle (unstable) and increasing fear level k to $k = 0.7$, $\tau = 1.98 > \tau_0$ system (3) becomes stable.

Remark 3. *With increase in fear level (k), the oscillatory behaviour of the system* (3) *induced by gestation delay settle down to stable dynamics. Thus, the fear level (k) has a stabilizing impact on the delay induced destabilization.*

6.3. Simulation results for the spatiotemporal system

In this subsection, we have presented the series of numerical simulations to explore the spatiotemporal dynamics of the system (56). Temporal part of the model system (56) is solved by using Euler's methods and five-point stencil finite difference scheme is used for diffusion part. All the numerical simulations employ the zero-flux boundary conditions on the domain of size 100×100. Space step and time step are taken as $\Delta h = 1$ and $\Delta t = 0.01$. Initial conditions are taken as small heterogeneous perturbations around the homogeneous steady state E^*. In all patterns, red color denotes the high population density and the blue color denotes the low population density of species. In these simulations, we have taken sufficiently large time to ensure the stationary patterns. We have verified the obtained spatial structures with different Δh and Δt.

In Example 5.1, we have shown that cross-diffusion induced Turing instability occurs in the system (56) for $d_{21} = 13.5 > d_{21}^{cr}$. Here, we investigate the spatial patterns due to Turing instability in the spatial system (56). At $d_{21} = 13.5$, remaining parameters are same as given in Example 5.1, hexagonal hot spot and cold spot patterns are observed (cf. Figs. 12(a) and 12(b)). This represent that, high density of prey species lies on the isolated hexagonal regions and remaining domain consists low density of prey species, whereas high density of predator species lies on the whole domain except the isolated hexagonal patches of low density.

Remark 4. *In these patterns high density regions of prey correspond to low density regions of predator. Thus, both populations are negatively correlated.*

In Fig. 13, we present the evolution process of hexagonal hot spot patterns shown in Fig. 12(a) taking time $t = 0$, 100, 300, 420, 460, 1000 days. Firstly, at $t = 300$ days, some hot spots appear in domain (cf. Fig. 13(c)) whose number increase at $t = 420$ days (cf. Fig. 13(d)). At $t = 460$ days, almost half domain is occupied with hexagonal hot spot patterns (cf. Fig. 13(e)) and finally at $t = 1000$ days hexagonal hot spot patterns spread over the entire domain (cf. Fig. 13(f)).

The effect of cross-diffusion coefficient of prey d_{12} on the pattern dynamics has been investigated in Fig. 14. For this, we have taken $d_2 = 0.01$ and $d_{21} = 13.5$., other system parameters are same as given in Example 5.1. At $d_{12} = 0.8$, hexagonal hot and cold spots appear (cf. Figs. 14(a) and (b)). These patterns goes to spots and stripes mixture at $d_{12} = 0.01$ (cf. Figs. 14(c) and (d)). Further, decreasing d_{12} to 0.001, labyrinthine patterns are obtained (cf. Figs. 14(e) and (f)).

7. Discussions and conclusions

It has been observed that predation threat significantly impact the phenotype and fitness of animals [44, 45, 13]. McCauley et al. [46] have reported that dragonflies survivorship reduced remarkably due to the mere presence of piscine predators [46]. Zanette et al. [16] have reported the 40% reduction in the number of offspring of song sparrows due to fear of predator alone. These experimental works suggested that fear is a crucial drive for changes in nature and elicits a vast array of responses spanning the physiology, morphology, and behavior of scared organisms [47, 48, 12, 49].

The cost of fear in the mathematical model of predator-prey interactions is first introduced by Wang et al. [17]. After this work, various studies have been carried out to understand the impact of fear on the predator-prey interactions and its trophic cascades on the lower trophic levels [20, 23, 39, 30, 29, 40]. In the present work, we have incorporated the cost of fear in the modified LG model with C-M functional response. We have studied the boundedness, equilibria, and stability analysis of the proposed system. It is found that periodic solutions of the temporal system go to a stable state with an increase in the fear level k. Also, prey and predator population densities decrease with an increase in the value of k.

We have incorporated the gestation delay in the proposed system for a more realistic formulation. The local stability of the delayed system is examined via Hopf-bifurcation. A critical value of gestation delay (τ) is obtained as $\tau_0 = 1.89157$. The system is stable if $\tau < \tau_0$, Hopf-bifurcation occurs at $\tau = \tau_0$ and system becomes unstable and remain unstable if $\tau > \tau_0$ (cf. Figs. 7 and 8). We have also derived the formulae for direction, stability, and period of bifurcation periodic solutions. It is obtained that Hopf-bifurcation occurring at $\tau = \tau_0 = 1.89157$ is supercritical (as $\mu_2 > 0$), bifurcating periodic solutions arising through Hopf-bifurcation are stable (as $\beta_2 < 0$) and their period increases with time (as $T_2 > 0$). To explore the impact of fear, we have plotted the bifurcation diagram with respect to the level of fear k, taking $\tau = 1.98$ from its instability region (cf. Fig. 10). With the increase in the value of k, the unstable dynamics of the system go to the stable state. Thus, fear level k has a stabilizing impact on the delay induced destabilization.

In this work, we have also studied the spatiotemporal extension of the proposed system (2) incorporating the self and nonlinear cross-diffusion terms. Turing instability conditions are derived and explored in Example 5.1. Analytical expression of Turing bifurcation threshold d_{21}^{cr} is obtained, whose numerical value is calculated as $d_{21}^{cr} = 12.782417$. Hexagonal hot and cold spot patterns appear for $d_{21} = 13.5 > d_{21}^{cr}$ (12). The evolution process of these patterns is shown in Fig. 13. It is found that the cross-diffusion coefficient of prey d_{12} also has a significant effect on pattern dynamics. Hexagonal spot patterns go to spots and stripes mixture and then to labyrinthine patterns with the change in the value of d_{12} (cf. Fig. 14). It is noticed that high-density regions of the prey population correspond to low-density regions of the predator population, this exhibits the negative correlation between the species. Another important observation is that fear level k has both stabilizing and destabilizing impact on nonlinear cross-diffusion induced Turing instability.

In this work, we have explored the effect of fear on temporal, delayed, and spatiotemporal dynamics of the predator-prey system. Nonlinear cross-diffusion is incorporated which is rarely investigated in the predator-prey model with fear effect. Our results may enrich the understanding of predator-prey system with the cost of fear.

References

[1] S. L. Lima, Nonlethal effects in the ecology of predator-prey interactions, Bioscience 48 (1998) 25–34.

[2] C. D. MacLeod, R. MacLeod, J. A. Learmonth, W. Cresswell, G. J. Pierce, Predicting population-level risk effects of predation from the responses of individuals, Ecology 95 (2014) 2006–2015.

[3] S. Creel, J. Winnie Jr., B. Maxwell, K. Hamlin, M. Creel, Elk alter habitat selection as an antipredator response to wolves, Ecology 86 (2005) 3387–3397.

[4] M. Hebblewhite, C. A. White, C. G. Nietvelt, J. A. McKenzie, T. E. Hurd, J. M. Fryxell, S. E. Bayley, P. C. Paquet, Human activity mediates a trophic cascade caused by wolves, Ecology 86 (2005) 2135–2144.

[5] D. Fortin, H. L. Beyer, M. S. Boyce, D. W. Smith, T. Duchesne, J. S. Mao, Wolves influence elk movements: behavior shapes a trophic cascade in Yellowstone National Park, Ecology 86 (2005) 1320–1330.

[6] O. J. Schmitz, A. P. Beckerman, K. M. O'Brien, Behaviorally mediated trophic cascades: effects of predation risk on food web interactions, Ecology 78 (1997) 1388–1399.

[7] M. J. Childress, M. A. Lung, Predation risk, gender and the group size effect: does elk vigilance depend upon the behaviour of conspecifics?, Animal behaviour 66 (2003) 389–398.

[8] O. HOGSTAD, Advantages of social foraging of Willow Tits Parus montanus, Ibis 130 (1988) 275–283.

[9] M. Díaz, A. P. Møller, E. Flensted-Jensen, T. Grim, J. D. Ibáñez-Álamo, J. Jokimäki, G. Markó, P. Tryjanowski, The geography of fear: a latitudinal gradient in anti-predator escape distances of birds across Europe, PloS one 8 (2013) e64634.

[10] S. L. Lima, P. A. Bednekoff, Temporal variation in danger drives antipredator behavior: the predation risk allocation hypothesis, Am. Nat. 153 (1999) 649–659.

[11] J. Winnie Jr., S. Creel, Sex-specific behavioural responses of elk to spatial and temporal variation in the threat of wolf predation, Animal behaviour 73 (2007) 215–225.

[12] E. L. Preisser, D. I. Bolnick, M. F. Benard, Scared to death? The effects of intimidation and consumption in predator–prey interactions, Ecology 86 (2005) 501–509.

[13] S. Creel, D. Christianson, Relationships between direct predation and risk effects, Trends Ecol. Evol. 23 (2008) 194–201.

[14] K. L. Pangle, S. D. Peacor, O. E. Johannsson, Large nonlethal effects of an invasive invertebrate predator on zooplankton population growth rate, Ecology 88 (2007) 402–412.

[15] B. L. Peckarsky, C. A. Cowan, M. A. Penton, C. Anderson, Sublethal consequences of stream-dwelling predatory stoneflies on mayfly growth and fecundity, Ecology 74 (1993) 1836–1846.

[16] L. Y. Zanette, A. F. White, M. C. Allen, M. Clinchy, Perceived predation risk reduces the number of offspring songbirds produce per year, Science 334 (2011) 1398–1401.

[17] X. Wang, L. Zanette, X. Zou, Modelling the fear effect in predator–prey interactions, J Math. Biol. 73 (2016) 1179–1204.

[18] J. Wang, Y. Cai, S. Fu, W. Wang, The effect of the fear factor on the dynamics of a predator-prey model incorporating the prey refuge, Chaos: An Interdisciplinary Journal of Nonlinear Science 29 (2019) 083109.

[19] H. Zhang, Y. Cai, S. Fu, W. Wang, Impact of the fear effect in a prey-predator model incorporating a prey refuge, Applied Mathematics and Computation 356 (2019) 328–337.

[20] X. Wang, X. Zou, Modeling the fear effect in predator–prey interactions with adaptive avoidance of predators, Bulletin of Mathematical Biology 79 (2017) 1325–1359.

[21] P. Panday, N. Pal, S. Samanta, J. Chattopadhyay, A three species food chain model with fear induced trophic cascade, International Journal of Applied and Computational Mathematics 5 (2019) 100.

[22] S. K. Sasmal, Population dynamics with multiple allee effects induced by fear factors–a mathematical study on prey-predator interactions, Applied Mathematical Modelling 64 (2018) 1–14.

[23] X. Wang, X. Zou, Pattern formation of a predator-prey model with the cost of anti-predator behaviors, Math. Biosci. Eng. 15 (????) 775–805.

[24] R. K. Upadhyay, S. Mishra, Population dynamic consequences of fearful prey in a spatiotemporal predator-prey system, Math. Biosci. Eng. 16 (2018) 338–372.

[25] J. P. Tripathi, S. Tyagi, S. Abbas, Global analysis of a delayed density dependent predator–prey model with crowley–martin functional response, Communications in Nonlinear Science and Numerical Simulation 30 (2016) 45–69.

[26] T. Liao, H. Yu, M. Zhao, Dynamics of a delayed phytoplankton-zooplankton system with crowley-martin functional response, Advances in Difference Equations 2017 (2017) 1–30.

[27] B. Roy, S. K. Roy, et al., Holling–tanner model with beddington–deangelis functional response and time delay introducing harvesting, Mathematics and Computers in Simulation 142 (2017) 1–14.

[28] R. K. Upadhyay, S. Mishra, Y. Dong, Y. Takeuchi, Exploring the dynamics of a tritrophic food chain model with multiple gestation periods, Mathematical biosciences and engineering: MBE 16 (2019) 4660–4691.

[29] P. Panday, S. Samanta, N. Pal, J. Chattopadhyay, Delay induced multiple stability switch and chaos in a predator–prey model with fear effect, Mathematics and Computers in Simulation 172 (2020) 134–158.

[30] A. Kumar, B. Dubey, Modeling the effect of fear in a prey–predator system with prey refuge and gestation delay, International Journal of Bifurcation and Chaos 29 (2019) 1950195.

[31] D. Duan, B. Niu, J. Wei, Hopf-hopf bifurcation and chaotic attractors in a delayed diffusive predator-prey model with fear effect, Chaos, Solitons & Fractals 123 (2019) 206–216.

[32] E. H. Kerner, A statistical mechanics of interacting biological species, The bulletin of mathematical biophysics 19 (1957) 121–146.

[33] E. H. Kerner, Further considerations on the statistical mechanics of biological associations, The bulletin of mathematical biophysics 21 (1959) 217–255.

[34] N. Shigesada, K. Kawasaki, E. Teramoto, Spatial segregation of interacting species, Journal of theoretical biology 79 (1979) 83–99.

[35] A. Madzvamuse, H. S. Ndakwo, R. Barreira, Cross-diffusion-driven instability for reaction-diffusion systems: analysis and simulations, Journal of mathematical biology 70 (2015) 709–743.

[36] G.-Q. Sun, Z. Jin, L. Li, M. Haque, B.-L. Li, Spatial patterns of a predator-prey model with cross diffusion, Nonlinear Dynamics 69 (2012) 1631–1638.

[37] Y. Cai, W. Wang, Stability and hopf bifurcation of the stationary solutions to an epidemic model with cross-diffusion, Computers & Mathematics with Applications 70 (2015) 1906–1920.

[38] M. Banerjee, S. Ghorai, N. Mukherjee, Study of cross-diffusion induced turing patterns in a ratio-dependent prey-predator model via amplitude equations, Applied Mathematical Modelling 55 (2018) 383–399.

[39] S. Mishra, R. K. Upadhyay, Strategies for the existence of spatial patterns in predator–prey communities generated by cross-diffusion, Nonlinear Analysis: Real World Applications 51 (2020) 103018.

[40] R. Han, L. N. Guin, B. Dai, Cross-diffusion-driven pattern formation and selection in a modified leslie–gower predator–prey model with fear effect, Journal of Biological Systems 28 (2020) 27–64.

[41] N. Ali, M. Jazar, Global dynamics of a modified leslie-gower predator-prey model with crowley-martin functional responses, Journal of Applied Mathematics and Computing 43 (2013) 271–293.

[42] H. Freedman, V. S. H. Rao, The trade-off between mutual interference and time lags in predator-prey systems, Bulletin of Mathematical Biology 45 (1983) 991–1004.

[43] B. D. Hassard, B. Hassard, N. D. Kazarinoff, Y.-H. Wan, Y. W. Wan, Theory and applications of Hopf bifurcation, volume 41, CUP Archive, 1981.

[44] J. Michaud, P. R. Barbosa, C. L. Bain, J. B. Torres, Extending the "ecology of fear" beyond prey: Reciprocal nonconsumptive effects among competing aphid predators, Environmental entomology 45 (2016) 1398–1403.

[45] S. L. Lima, L. M. Dill, Behavioral decisions made under the risk of predation: a review and prospectus, Canadian journal of zoology 68 (1990) 619–640.

[46] S. J. McCauley, L. Rowe, M.-J. Fortin, The deadly effects of "nonlethal" predators, Ecology 92 (2011) 2043–2048.

[47] L. B. Kats, L. M. Dill, The scent of death: chemosensory assessment of predation risk by prey animals, Ecoscience 5 (1998) 361–394.

[48] W. W. Weisser, C. Braendle, N. Minoretti, Predator-induced morphological shift in the pea aphid, Proceedings of the Royal Society of London. Series B: Biological Sciences 266 (1999) 1175–1181.

[49] E. H. Nelson, C. E. Matthews, J. A. Rosenheim, Predators reduce prey population growth by inducing changes in prey behavior, Ecology 85 (2004) 1853–1858.

Appendix

$p_1 = -d + \frac{w\alpha y^*}{(1+\alpha x^*)^3(1+\beta y^*)}$, $p_2 = -\frac{ak}{(1+ky^*)^2} - \frac{w}{(1+\alpha x^*)^2(1+\beta y^*)^2}$,
$p_3 = \frac{ak^2x^*}{(1+ky^*)^3} + \frac{w\beta x^*}{(1+\alpha x^*)(1+\beta y^*)^3}$, $p_4 = -\frac{hy^{*2}}{(x^*+b)^3}$, $p_5 = \frac{2hy^*}{(x^*+b)^2}$, $p_6 = -\frac{h}{(x^*+b)}$.

Determination of values of E_1 and E_2

From the definition of A and Eqs. (45), (46) that

$$\int_{-1}^{0} W_{20}(\theta)d\eta(\theta) = 2i\omega_0\tau_0 W_{20}(0) - H_{20}(0), \tag{72}$$

and

$$\int_{-1}^{0} W_{11}(\theta)d\eta(\theta) = -H_{11}(0), \tag{73}$$

where $\eta(\theta) = \eta(0,\theta)$. From Eqs. (41) and (43), we have

$$H_{20}(0) = -g_{20}q(0) - \bar{g}_{02}\bar{q}(0) + 2\tau_0 \begin{pmatrix} p_1 + p_2\alpha_2 + p_3\alpha_2^2 \\ (p_4 + p_5\alpha_2 + p_6\alpha_2^2)e^{-2i\omega_0\tau_0} \end{pmatrix} \tag{74}$$

and

$$H_{11}(0) = -g_{11}q(0) - \bar{g}_{11}\bar{q}(0) + \tau_0 \begin{pmatrix} 2p_1 + 2p_2\mathrm{Re}(\alpha_2) + 2p_3\bar{\alpha}_2\alpha_2 \\ 2p_4 + 2p_5\mathrm{Re}(\alpha_2) + 2p_6\bar{\alpha}_2\alpha_2 \end{pmatrix}. \tag{75}$$

Using Eqs. (51) and (74) in Eq. (72) and noticing that

$$\left\{i\omega_0\tau_0 I - \int_{-1}^{0} e^{i\omega_0\tau_0\theta} d\eta(\theta)\right\} q(0) = 0, \tag{76}$$

and

$$\left\{-i\omega_0\tau_0 I - \int_{-1}^{0} e^{-i\omega_0\tau_0\theta} d\eta(\theta)\right\} \bar{q}(0) = 0, \tag{77}$$

we obtained that

$$\left\{2i\omega_0\tau_0 I - \int_{-1}^{0} e^{2i\omega_0\tau_0\theta} d\eta(\theta)\right\} E_1 = 2\tau_0 \begin{pmatrix} p_1 + p_2\alpha_2 + p_3\alpha_2^2 \\ (p_4 + p_5\alpha_2 + p_6\alpha_2^2)e^{-2i\omega_0\tau_0} \end{pmatrix}, \tag{78}$$

This leads to

$$\begin{pmatrix} 2i\omega_0 - a_1 & -a_2 \\ -b_1 e^{-i\omega_0\tau_0} & 2i\omega_0 - s - b_2 e^{-i\omega_0\tau_0} \end{pmatrix} E_1 = 2 \begin{pmatrix} p_1 + p_2\alpha_2 + p_3\alpha_2^2 \\ (p_4 + p_5\alpha_2 + p_6\alpha_2^2)e^{-2i\omega_0\tau_0} \end{pmatrix}, \tag{79}$$

Solving above system for E_1, we obtain

$$E_1^{(1)} = \frac{2}{\widetilde{A}} \begin{vmatrix} p_1 + p_2\alpha_2 + p_3\alpha_2^2 & -a_{12} \\ (p_4 + p_5\alpha_2 + p_6\alpha_2^2)e^{-2i\omega_0\tau_0} & 2i\omega_0 - s - b_{22}e^{-i\omega_0\tau_0} \end{vmatrix},$$

$$E_1^{(2)} = \frac{2}{\widetilde{A}} \begin{vmatrix} 2i\omega_0 - a_{11} & p_1 + p_2\alpha_2 + p_3\alpha_2^2 \\ -b_{21}e^{-i\omega_0\tau_0} & (p_4 + p_5\alpha_2 + p_6\alpha_2^2)e^{-2i\omega_0\tau_0} \end{vmatrix},$$

where

$$\widetilde{A} = \begin{vmatrix} 2i\omega_0 - a_{11} & -a_{12} \\ -b_{21}e^{-i\omega_0\tau_0} & 2i\omega_0 - s - b_{22}e^{-i\omega_0\tau_0} \end{vmatrix}.$$

Similarly, substituting Eqs. (52) and (75) in Eq. (72), we obtain

$$\begin{pmatrix} -a_{11} & -a_{12} \\ -b_{21}e^{-i\omega_0\tau_0} & -s - b_{22}e^{-i\omega_0\tau_0} \end{pmatrix} E_2 = \begin{pmatrix} 2p_1 + 2p_2\mathrm{Re}(\alpha_2) + 2p_3\bar{\alpha}_2\alpha_2 \\ 2p_4 + 2p_5\mathrm{Re}(\alpha_2) + 2p_6\bar{\alpha}_2\alpha_2 \end{pmatrix},$$

and hence

$$E_2^{(1)} = \frac{2}{\widetilde{B}} \begin{vmatrix} p_1 + p_2\mathrm{Re}(\alpha_2) + p_3\bar{\alpha}_2\alpha_2 & -a_{12} \\ p_4 + p_5\mathrm{Re}(\alpha_2) + p_6\bar{\alpha}_2\alpha_2 & -s - b_{22}e^{-i\omega_0\tau_0} \end{vmatrix},$$

$$E_2^{(2)} = \frac{2}{\widetilde{B}} \begin{vmatrix} -a_{11} & p_1 + p_2\mathrm{Re}(\alpha_2) + p_3\bar{\alpha}_2\alpha_2 \\ -b_{21}e^{-i\omega_0\tau_0} & p_4 + p_5\mathrm{Re}(\alpha_2) + p_6\bar{\alpha}_2\alpha_2 \end{vmatrix},$$

where

$$\widetilde{B} = \begin{vmatrix} -a_{11} & -a_{12} \\ -b_{21}e^{-i\omega_0\tau_0} & -s - b_{22}e^{-i\omega_0\tau_0} \end{vmatrix}.$$

Tables and Figures

Table 1: Biological meanings of the parameters used in the system (1).

Parameters	Definitions
a	Intrinsic growth rate of prey population
d	Death rate of prey due to intra-specific competition
w	Effect of capture rate
α	Handling time of prey by the predator
β	The magnitude of interference among predators
s	Growth rate of predator y
h	Maximum value which per capita reduction rate of y can attain
b	Extent to which the environment provides protection to species y

Table 2: Number of possible positive real roots of Eq. (9)

Cases	P_4	P_3	P_2	P_1	P_0	Number of sign changes	Number of possible positive real roots (E^*)
1	+	+	+	+	+	0	0
2	+	+	−	+	+	2	0, 2
3	+	+	+	−	+	2	0, 2
4	+	+	+	+	−	1	1
5	+	+	−	−	+	2	0, 2
6	+	+	+	−	−	1	1
7	+	+	−	+	−	3	1, 3
8	+	+	−	−	−	1	1

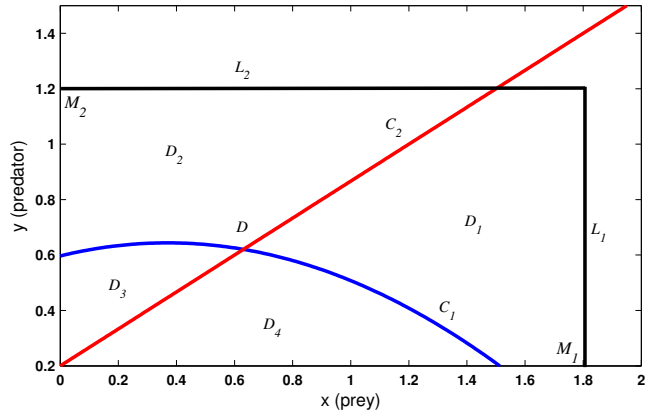

Figure 1: Phase portrait of the system (2) in $x - y$ plane with parameter set $a = 1.4,\ k = 0.01,\ d = 0.8,\ w = 2.36,\ \alpha = 1,\ \beta = 0.02,\ s = 0.1,\ h = 0.15,\ b = 0.3$.

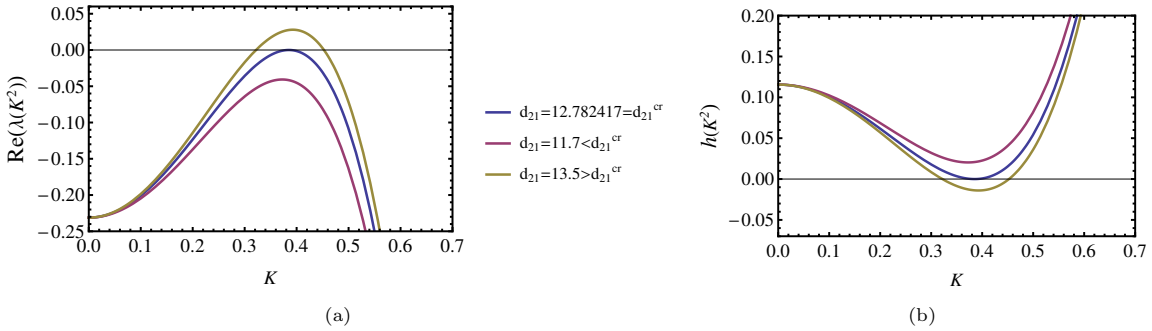

(a) (b)

Figure 2: (a) $\mathrm{Re}(\lambda(K^2))$ vs. K plot. (b) $h(K^2)$ vs. K plot for different d_{21}. (For interpretation of the references to color in this figure legend, the reader is referred to the web version of this article.)

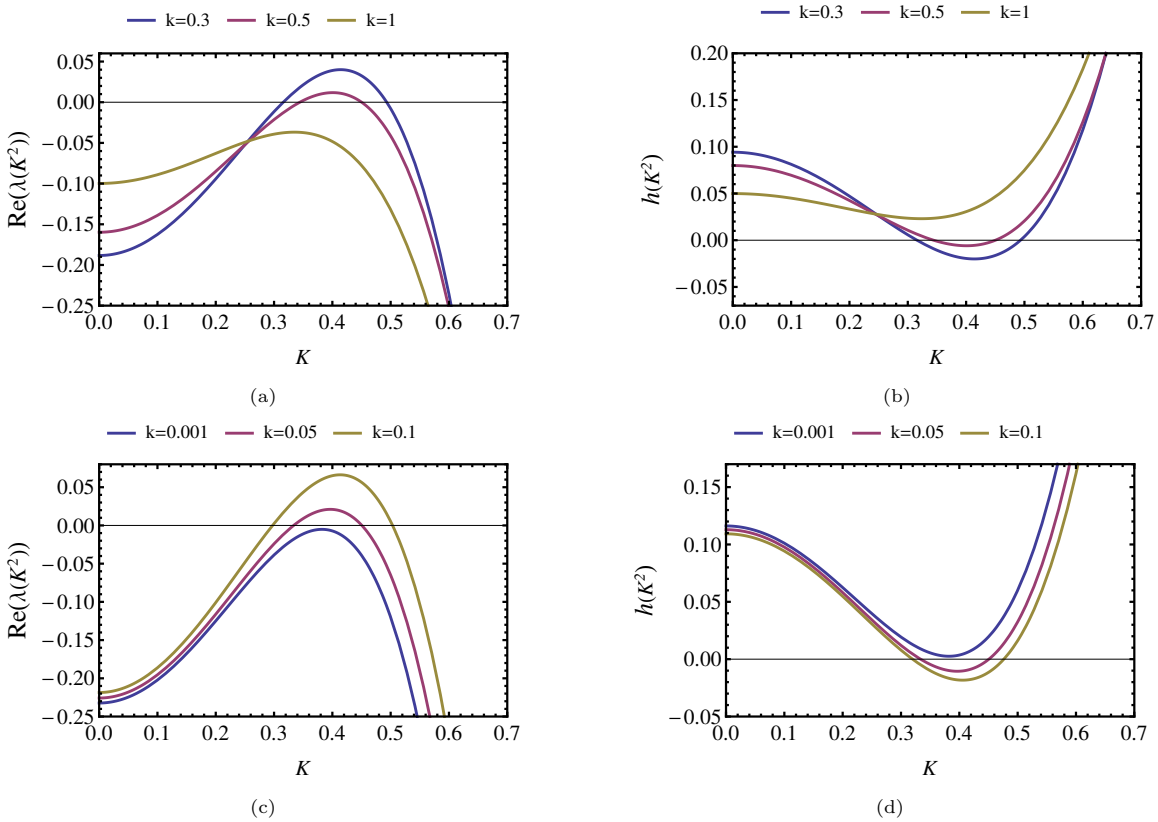

(a) (b) (c) (d)

Figure 3: (a) Graph of $\mathrm{Re}(\lambda(K^2))$ vs. K. (b) $h(K^2)$ vs. K for $k = 0.3,\ 0.5,\ 1$. (c) Graph of $\mathrm{Re}(\lambda(K^2))$ vs. K. (d) $h(K^2)$ vs. K for $k = 0.001,\ 0.05,\ 0.1$. $d_{21} = 12.8$ and other parameters remain same as given in Example 5.1. (For interpretation of the references to color in this figure legend, the reader is referred to the web version of this article.)

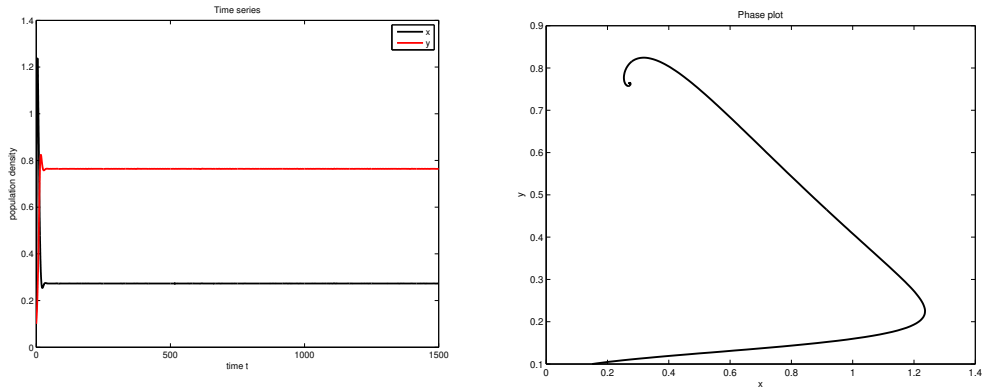

(a) (b)

Figure 4: (a) Time series plot for prey and predator populations, (b) phase portrait in xy-plane for the system (2).

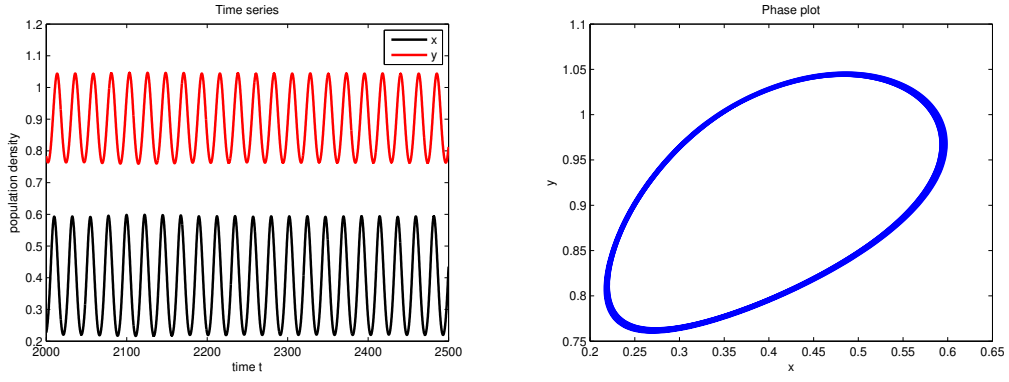

(a) (b)

Figure 5: (a) Time series at $\alpha = 2.4$ and $\beta = 0.002$, periodic oscillations. (b) Phase diagram at $\alpha = 2.4$ and $\beta = 0.002$, limit cycle. Other parameter are same as given in (71).

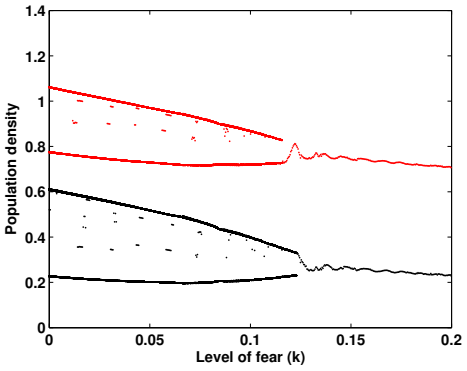

(a)

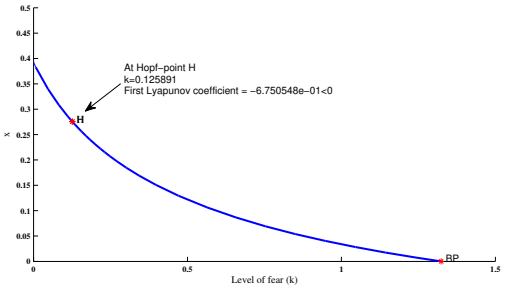

(b)

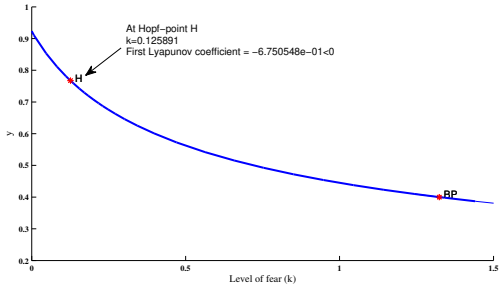

(c)

Figure 6: (a) Bifurcation diagram of the system (2) taking level of fear k as a control parameter. (b),(c) Prey and predator biomass as a function of fear level k.

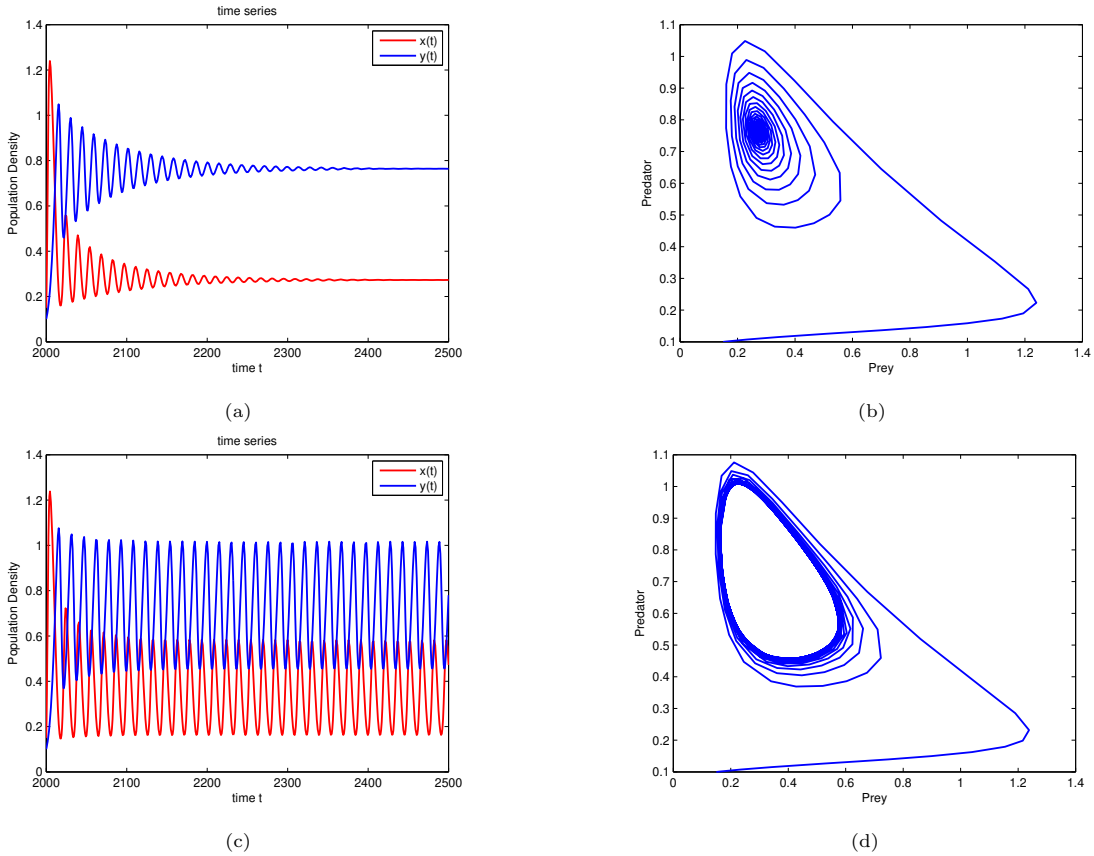

Figure 7: Time series and phase diagram of the system (3) at (a),(b) $\tau = 1.82 < \tau_0 = 1.89157$, stable focus, (c),(d) $\tau = 1.94 > \tau_0 = 1.89157$, limit cycle. System parameters are same as given in (71).

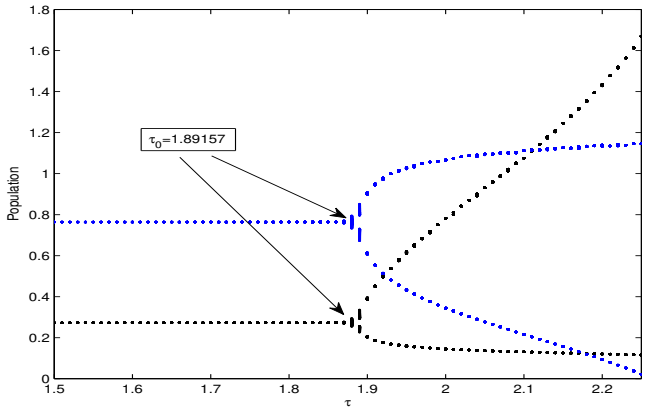

Figure 8: Bifurcation diagram of system (3) w.r.t. gestation delay τ in the range $\tau \in [1.5, 2.25]$. Showing that the system (3) is stable for $\tau < \tau_0 = 1.89157$ and unstable for $\tau > \tau_0 = 1.89157$. Hopf-bifurcation occurs at $\tau = \tau_0 = 1.89157$.

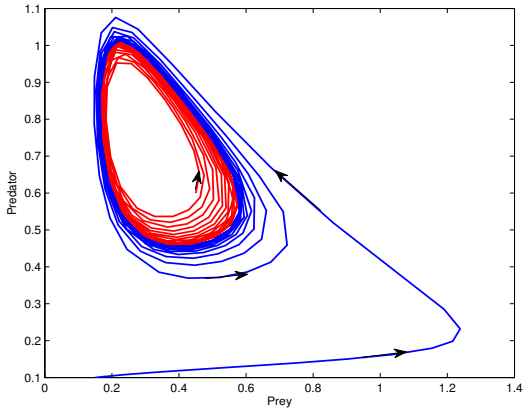

Figure 9: Two solution trajectories starting with different initial conditions for $\tau = 1.94$, other parameter values are same as given in (71).

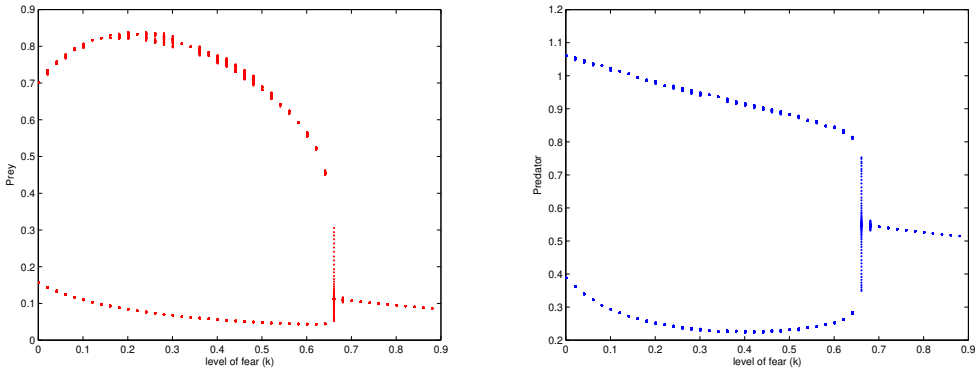

Figure 10: Bifurcation diagram of prey x and predator y w.r.t. fear level (k) in the range $k \in [0, 0.9]$, taking gestation delay $\tau = 1.98 > \tau_0$.

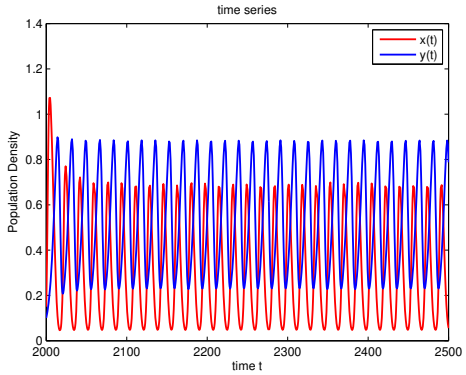

(a)

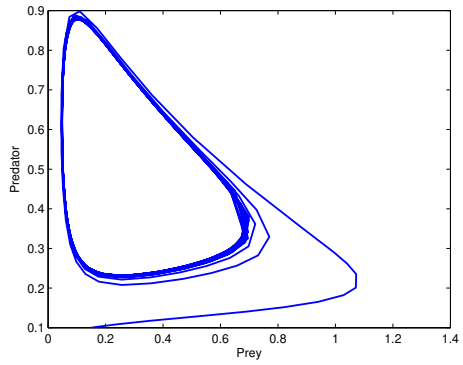

(b)

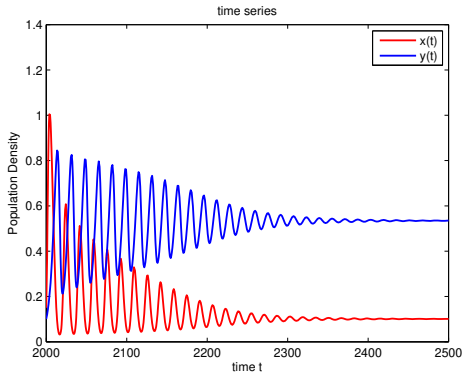

(c)

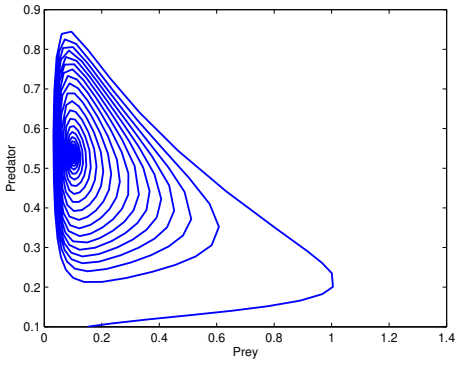

(d)

Figure 11: (a),(b) Time series, phase plot of the system (3) at $k = 0.5$ $\tau = 1.98$, showing oscillatory behaviour. (c),(d) Time series, phase plot of the system (3) at $k = 0.7$, showing stable dynamics. Other parameters are same as taken in (71).

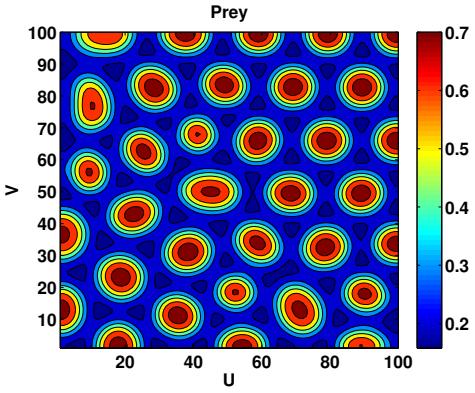

(a)

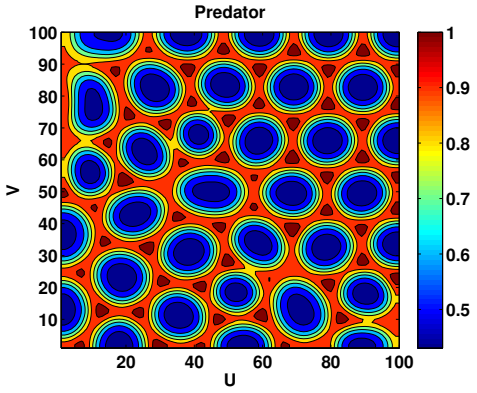

(b)

Figure 12: (a),(b)Snapshots of Turing patterns for parameters (70) with $d_{21} = 13.5$ at 2000 days.

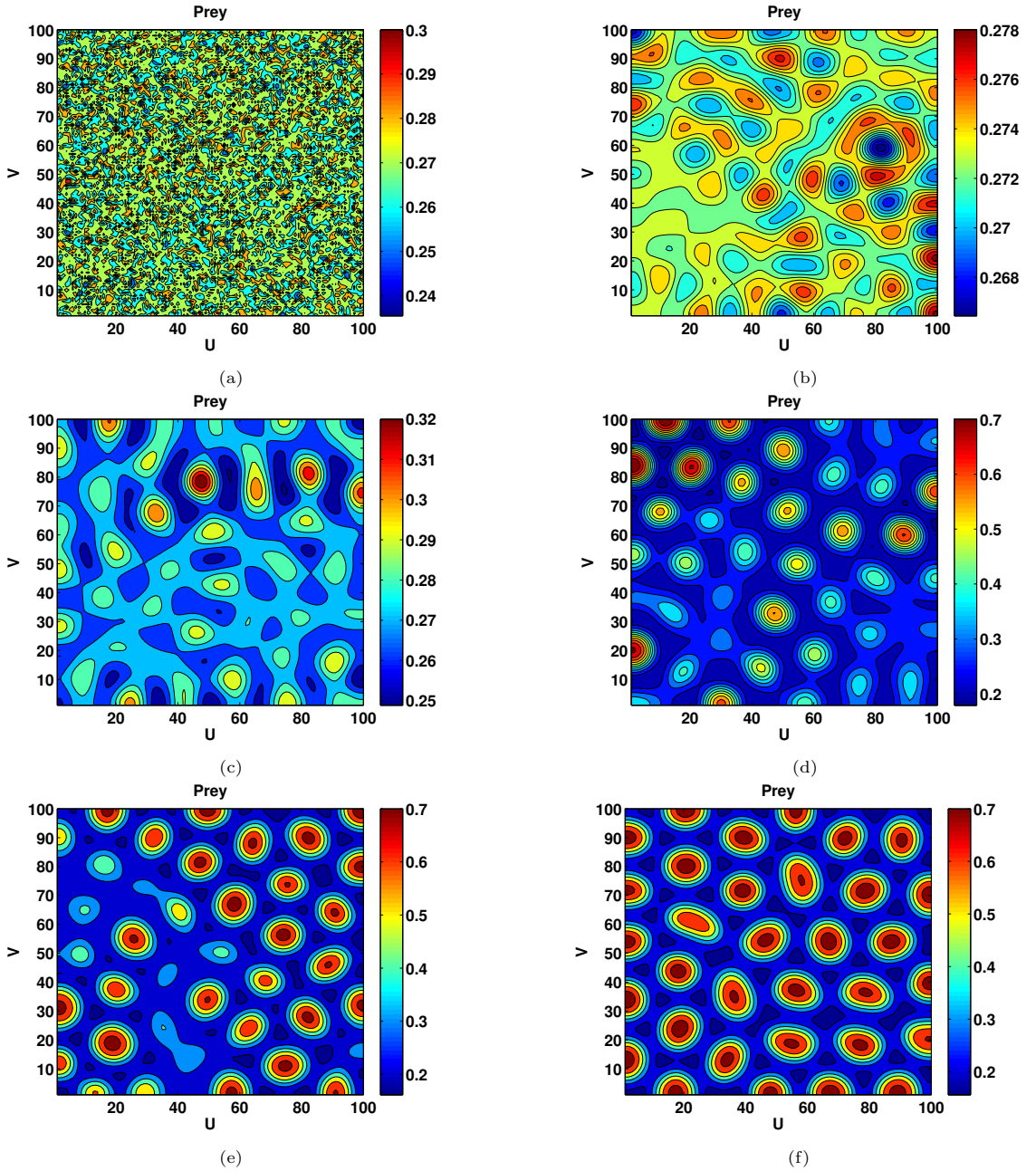

Figure 13: Snapshots of contour pictures of the time evolution of prey species at (a) $t = 0$ (b) $t = 100$ (c) $t = 300$ (d) $t = 420$ (e) $t = 460$ (f) $t = 1000$ days. For system parameters (70) with $d_{21} = 13.5$.

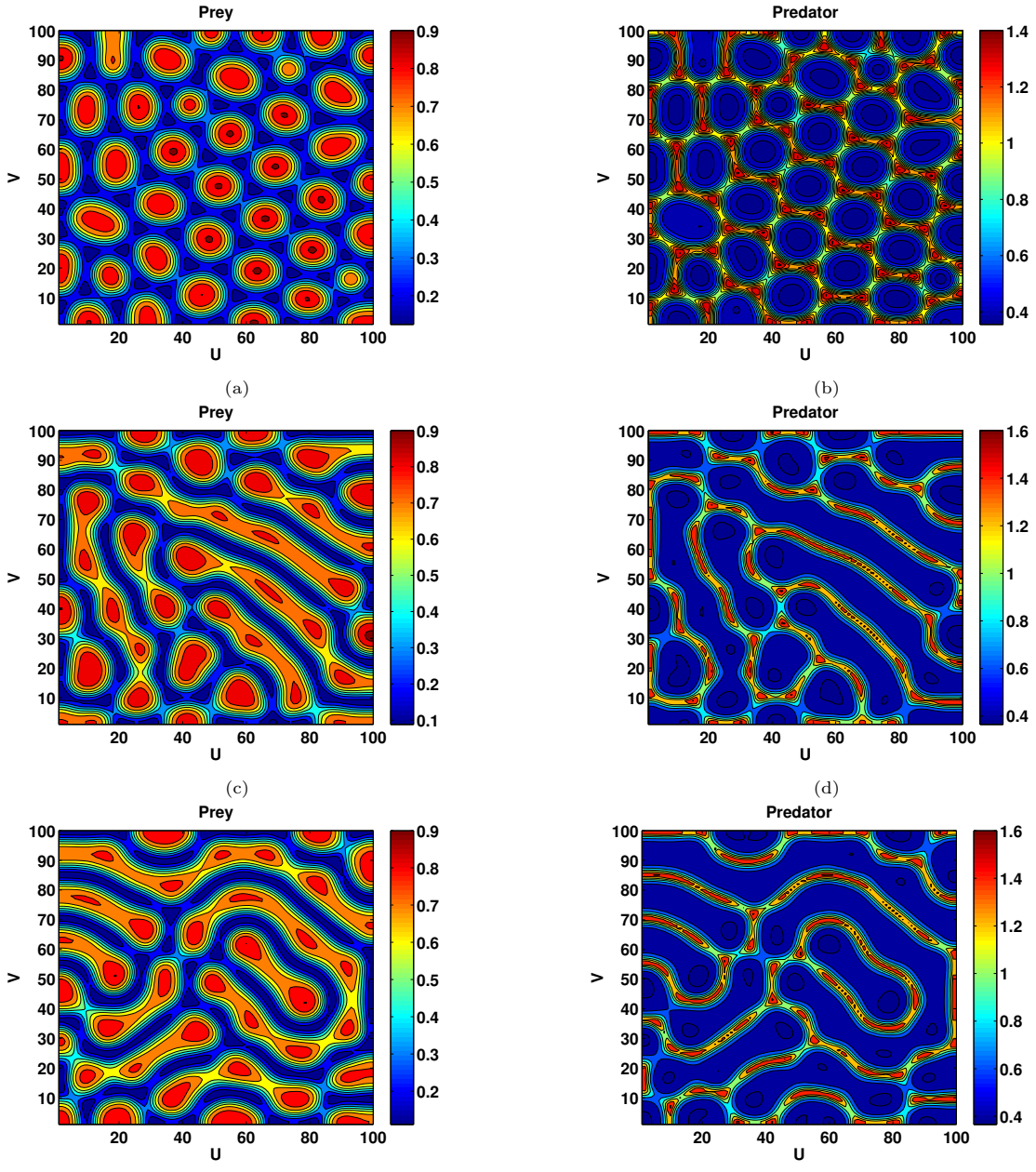

Figure 14: Snapshots of Turing patterns for different values of d_{12} at 1500 days (a) $d_{12} = 0.8$ (b) $d_{12} = 0.01$ (c) $d_{12} = 0.001$. Here $d_2 = 0.01$, $d_{21} = 13.5$ and remaing paraameters are same as given in Example 5.1.